Atmospheric Research 326 (2025) 108266

Contents lists available at ScienceDirect

Atmospheric Research

journal homepage: www.elsevier.com/locate/atmosres

Western Mediterranean flash floods through the Lens of Alcanar (NE Iberian Peninsula): Meteorological drivers and trends

Maria Carmen Llasat [a,b,*], Raül Marcos-Matamoros [a,c], Ramón Pascual [d], Tomeu Rigo [e], Damián Insúa-Costa [f], Alfredo Crespo-Otero [g]

[a] GAMA, Department of Applied Physics, Universitat de Barcelona, c) Martí Franqués 1, 08028 Barcelona, Spain
[b] Water Research Institute, Universitat de Barcelona, c) Martí Franqués 1, 08028 Barcelona, Spain
[c] Earth Sciences Department, Barcelona Supercomputing Center - CNS, Plaça d'Eusebi Güell, 1-3, Barcelona 08034, Spain
[d] Delegación de Barcelona, AEMET, c) Arquitecte Sert 1, 08005 Barcelona, Spain
[e] Servei Meteorològic de Catalunya, Área de Predicció Barcelona, c) Dr. Roux 80, 08017 Barcelona, Spain
[f] Hydro-Climate Extremes Lab, Ghent University, Coupure Links 653, 9000 Ghent, Belgium
[g] CRETUS, Non-linear Physics Group, Universidade de Santiago de Compostela, Rúa de José María Suárez Núñez, s/n, 15782 Santiago de Compostela, A Coruña, Spain

ARTICLE INFO

Keywords:
Flash floods
Heavy rainfalls
Extreme rainfalls
Moisture tracking
DANA
Mediterranean region
Alcanar

ABSTRACT

Flash floods in the Western Mediterranean pose a growing hazard due to the effects of climate change, rapid urbanization, and land-use changes. This study focuses on flash floods in the Montsià region of southern Catalonia (NE Iberian Peninsula), with particular emphasis on the municipality of Alcanar, because it illustrates the recent intensification of flash flood dynamics in the Western Mediterranean. The research is motivated by three recent severe flood events in Alcanar (2018, 2021, and 2023), each characterized by extraordinary rainfall totals and significant economic losses, unprecedented in the municipality's 30-year observational record. Methodologically, we integrate multiple data sources—including meteorological station observations, weather radar products, lightning detection networks, high-resolution mesoscale model outputs, and a flood database spanning 1980–2023, complemented by economic compensation records from 1996 to 2020. Through this approach we (i) assess the regional frequency of heavy rainfall and flood episodes, (ii) quantify the economic impacts in Alcanar, (iii) characterize the meteorological and thermodynamic conditions on the three most intense recent events (including moisture source tracking via a Lagrangian methodology), and (iv) analyze spatio-temporal trends in extreme rainfall indicators (percentiles, threshold exceedances, kurtosis, and skewness). Our findings suggest that, from a meteorological perspective, current flash flood behavior in the Western Mediterranean likely emerges from the interplay of localized orographic triggers, elevated sea surface temperatures, strong instability associated with low-level moisture, particular positioning of jet streaks, synoptic-scale cut-off lows, and remote moisture sources. The results also point to an increase in rainfall intensity, explained by the presence of high precipitable water content and shallow convection, which enhances precipitation efficiency. These insights highlight the critical need for robust flood early warning systems, strategic watershed management, and improved risk communication to mitigate escalating flash flood risks in the Montsià county and similar areas throughout the Western Mediterranean region.

1. Introduction

According to the latest IPCC report (IPCC, 2022), climate hazards are expected to increase globally, creating significant risks for ecosystems and human populations (very high confidence). At the same time, the World Meteorological Organization (WMO, 2023) notes that the frequency of recorded disasters has already increased fivefold in the last 50 years. Among these hazards, floods have also shown a marked increase, with a global rise documented across various latitudinal bands between 1985 and 2015 (Najibi and Devineni, 2018). In terms of their impacts, floods from 2000 to 2019 resulted in around US$650 billion in economic damage, affected 1.65 billion people, and led to more than 100,000 fatalities (United Nations, 2023). Looking forward, the IPCC (2022) predicts that the rising frequency and intensity of heavy precipitation

* Corresponding author at: GAMA, Department of Applied Physics, Universitat de Barcelona, c) Martí Franqués 1, 08028 Barcelona, Spain.
E-mail address: carmell@meteo.ub.edu (M.C. Llasat).

https://doi.org/10.1016/j.atmosres.2025.108266
Received 15 March 2025; Received in revised form 24 May 2025; Accepted 3 June 2025
Available online 16 June 2025

events (high confidence) will likely exacerbate localized, rain-induced flooding (medium confidence). Addressing these risks effectively requires a combination of structural and non-structural measures.

As highlighted by the IPCC (2022), early warning systems and resilient infrastructure are effective in minimizing harm to human lives and enhancing economic and social resilience by lowering vulnerability to hazards. Therefore, in March 2023, the United Nations (UN), with support from the WMO, launched the "*Early Warnings for All*" initiative, a global effort to ensure that every person on Earth is protected by early warning systems by 2027 (WMO, 2023). These systems are designed to be comprehensive and end-to-end, encompassing all stages from hazard monitoring, forecasting, and prediction to the critical final step: enabling effective responses at both individual and societal levels. Achieving this requires robust disaster risk assessments, efficient communication channels, and well-prepared communities capable of mitigating and adapting to the impacts of these events.

Reflecting the global challenges linked to flood hazard, flash floods remain a major concern in the Mediterranean region, as illustrated by the devastating events in Valencia (Spain) in October 2024. These episodes frequently occur in small, torrential coastal basins (Braud et al., 2014; Gaume et al., 2016), where the combination of their sudden onset and intense rainfall significantly complicates effective management. Adding to these difficulties, the First Mediterranean Assessment Report (MedECC, 2020) states that Northern Mediterranean countries face escalating risks in flood-prone areas due to rapid urbanization and increasing population densities, which exacerbate existing vulnerabilities.

In parallel, several studies have suggested a potential increase in flash flood events across different Mediterranean regions (Llasat et al., 2013; Tramblay et al., 2019; Faccini et al., 2021). This rise is attributed to both non-climatic factors—such as the already mentioned growing population, increased exposure of assets, and land-use changes (Hall et al., 2014; Gaume et al., 2016)—and climatic factors, including an uptick in short-duration heavy rainfalls, which are the primary triggers of flash floods (Llasat et al., 2021; Treppiedi et al., 2021). These findings align with earlier projections by Tramblay and Somot (2018), which anticipated an increase in heavy rainfall events in the northern Mediterranean, further confirmed by convective parameterization studies in areas like southern France (Poncet et al., 2024).

However, while heavy rains causing flash floods in Mediterranean coastal areas are frequent, predicting their exact location and providing timely warnings to the population is particularly difficult. This complexity stems from the Mediterranean's unique geographical and climatic characteristics—a closed, warm sea surrounded by mountains and subject to the influence of both subtropical and polar air masses—which create ideal conditions for convection at different scales and the rapid ascent of humid air (Romero et al., 1999; Llasat, 2009; Jansa et al., 2014). In fact, research by Insua-Costa et al. (2018, 2022) has shown that more than 40 % of the humidity contributing to heavy rainfall in the northwest Mediterranean can originate from distant extra-Mediterranean regions (i.e. the Atlantic Ocean). This accounts for the exceptional rainfall totals observed over short periods in some areas, such as the 600 mm recorded within 24 h in the Gard region of southeastern France in 2002 (Braud et al., 2010). These events are typically linked to synoptic and mesoscale conditions that promote vertical forcing, convergence of substantial water vapor from multiple domains, and the persistence of rainfall over localized areas.

Modern weather forecasting systems are generally capable of identifying these broader conditions and predicting them up to 24 h in advance. However, obstacles remain, especially in forecasting the precise location of rainfall maxima due to inherent uncertainties in the models. The situation becomes even more difficult in the case of highly convective episodes, which are shorter, more localized, and often produce catastrophic impacts. This complexity is particularly evident in the quantitative prediction of convective precipitation, including both its intensity and total accumulation, which are influenced by several interrelated factors: (1) the efficiency of precipitation processes that depends on drivers such as moisture content, microphysical characteristics, and the intensity of updrafts; (2) the interaction between atmospheric stability and triggers determining updraft formation; and (3) the movement and organization of convective cells, along with rainfall intensity. As a result, quantitative forecasts are influenced by uncertainties in each of these variables, which become progressively more pronounced as the prediction horizon lengthens.

Within this framework, this research seeks to strengthen flood early warning systems in the northwestern Mediterranean by characterizing the meteorological conditions that produce heavy rainfall and flash floods in Montsià county (southern Catalonia). Despite its small size, the region exemplifies the challenges faced along much of the Mediterranean coast, where tourism and holiday activities in flood-prone areas pose serious threats to human lives. The problem is compounded by limited awareness of the region's high flood risk, which is why its frequency and socioeconomic impacts are also analyzed. This reality is sharply illustrated by the case of Alcanar, which has suffered three catastrophic flood events in the past six years, each triggered by isolated, intense rainfall episodes that challenged forecasting capabilities and stand among the most severe in the municipality's 30-year observational record.

Hence, the article begins by exploring the complexities of the target area, providing an analysis of the climatic context of heavy rainfall in the region. This includes an examination of return periods and a characterization of significant rainfall events over the past 33 years. It then conducts a detailed analysis of the three most severe flooding episodes in the 30-year period (recorded in the last six years), adopting a meteorological perspective that spans from identifying moisture sources to analyzing convection processes. Based on this analysis, a conceptual model is proposed to enhance the understanding of these events. Finally, the article examines trends in intense rainfall and flooding within the region, assessing whether these patterns align with the anticipated impacts of climate change.

2. The study area

The county of Montsià, covering an area of 733 km^2, is the southernmost county in Catalonia (Fig. 1). It is defined by the "Serra del Montsià," a mountain range running southwest to northeast, reaching an elevation of 764 m above sea level, and lying close and parallel to the coastline (Fig. 2). This range, the highest entirely within the county, also lends its name to the region.

Although modest in size—spanning approximately 12 km in length and 5 km in width—the range is distinguished by its abrupt calcareous topography, characterized by cliffs, crags, and ravines. These geological features give rise to numerous steep torrents, locally known as *barrancs*. Moreover, the mountain range plays an essential role in lifting humid air masses from the Mediterranean, especially when the air flows perpendicularly to its axis. This interaction often triggers convection, resulting in episodes of intense rainfall. This combination of the range's steep torrents and heavy rainfall creates ideal conditions for frequent flash floods.

The county is bordered to the north by the Ebro River (Fig. 2), which is part of the hydrographic demarcation of the Ebro River Basin (CHE) (Fig. 3), and to the south by the Sénia River, within the Xúquer River Basin (CHX). Between these two basins lies a third area managed by the Internal Basins of Catalonia (CIC), creating a hydrographic landscape divided among three different administrative units. Alcanar, like other municipalities in the county, belongs to multiple hydrographic demarcations—in this case, the CHX and CIC. This coastal municipality is crossed by numerous torrents, around which urban development has significantly expanded, particularly due to the proliferation of second homes and campsites, resulting in an increase in population density in flood-prone areas.

Therefore, Montsià -and particularly the municipality of Alcanar-

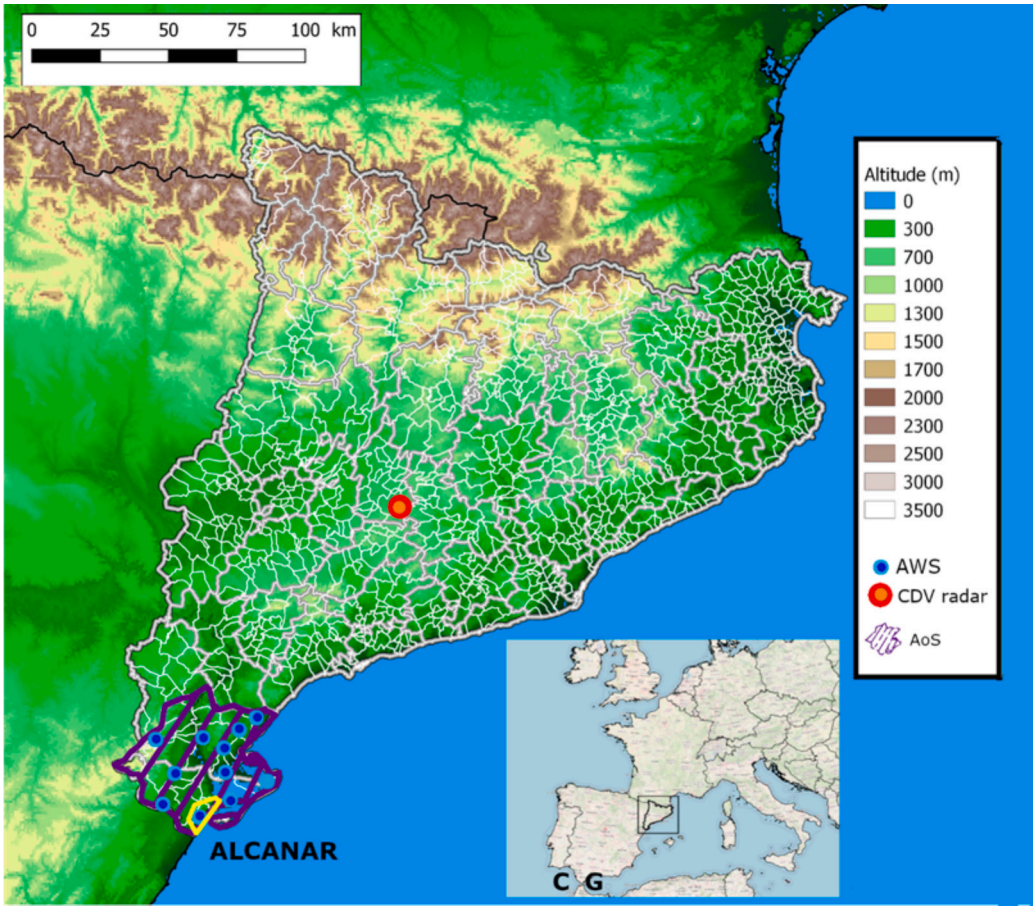

Fig. 1. Orographic map of Catalonia showing the locations of Baix Ebre and Montsià counties (Area of Study, AoS, shaded), XEMA network meteorological stations within these counties (blue circles, AWS), the SMC meteorological radar at La Panadella (red circle, CDV), and Alcanar municipality (yellow). The Strait of Gibraltar (G) and Cape San Vicente (C), referenced in the text, are also shown. (For interpretation of the references to colour in this figure legend, the reader is referred to the web version of this article.)

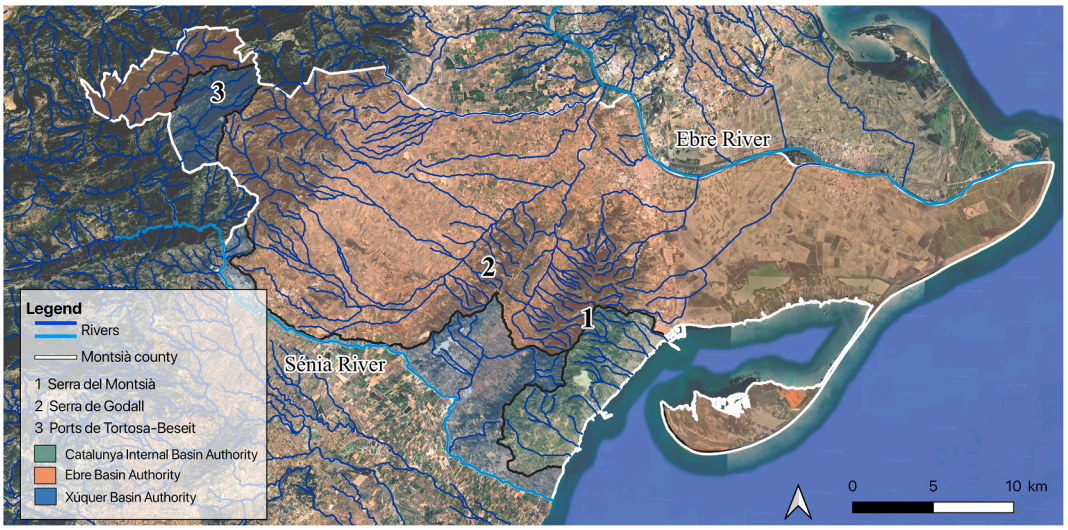

Fig. 2. Hydrographic and orographic map of Montsià county (white line), showing the Sénia River, the Ebro River, the Montsià range (Serra del Montsià) (1), the Godall range (Serra de Godall) (2), and the mountain range of Els Ports de Tortosa-Beseit (3). The sectors belonging to the different hydrographic basins are shown in different colors. Elaborated from Google maps.

exemplifies the urging need to enhance flood early warning systems and expand flood-related knowledge in the Mediterranean context. As we have seen, this need arises from three key factors: 1) a high flash flood hazard driven by the region's distinct geomorphological and climatic conditions; 2) significant flood exposure, especially along the coast, where socio-economic development in flood-prone areas has led to

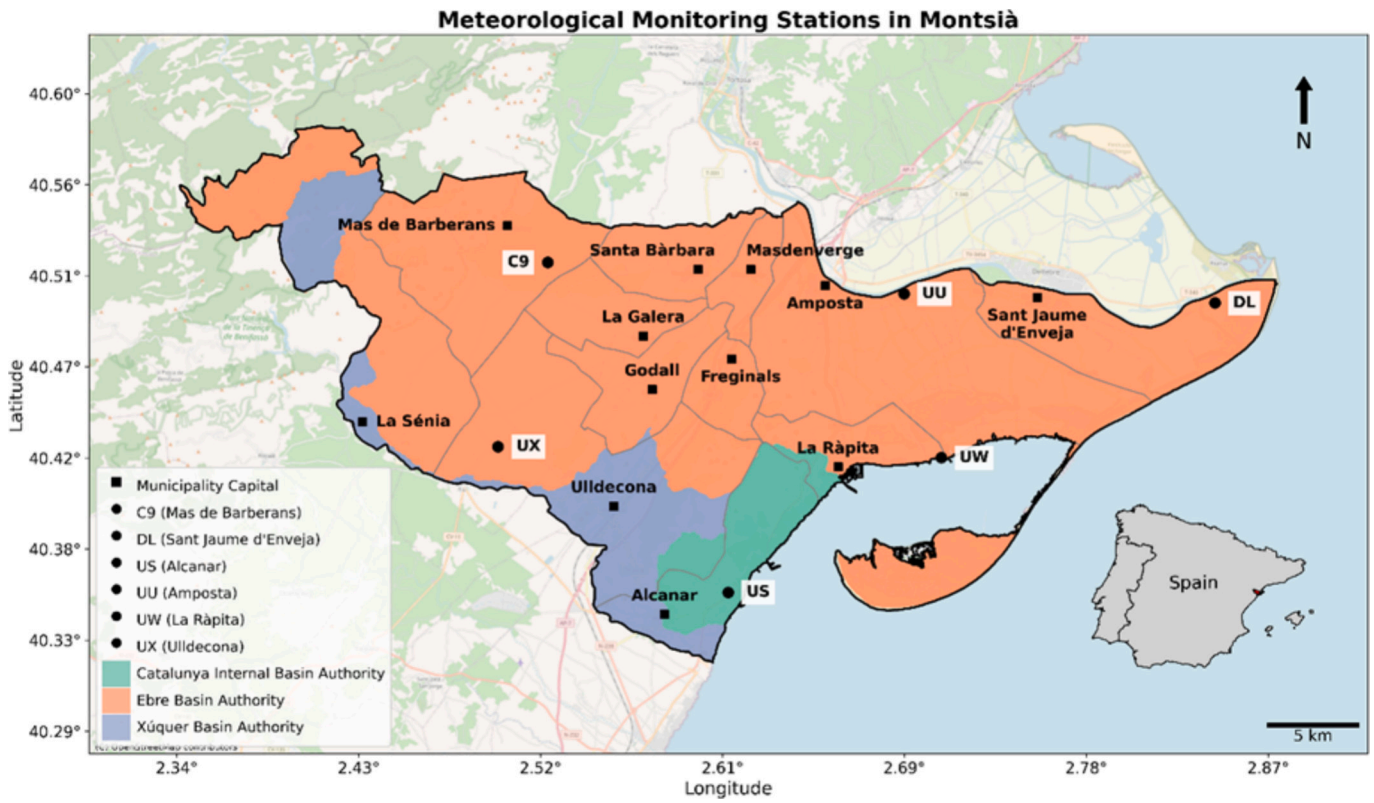

Fig. 3. Division of Montsià county into three hydrographic basins, indicating the locations of XEMA meteorological stations (circles) and municipal capitals (squares).

higher population densities; and 3) substantial flood vulnerability, stemming from a complex hydrographic management system involving up to three different water administrations, which complicates the implementation of preventive measures, combined with low public and individual risk awareness and the inherent challenges of accurately predicting and nowcasting flash floods.

3. Data sources

The rainfall data comes from the XEMA network ("Xarxa d'Estacions Meteorològiques Automàtiques," or Network of Automatic Meteorological Stations), which includes 189 stations, six of them located in Montsià county, including one in the municipality of Alcanar. All stations have been used to characterize the precipitation field of the three case studies, whereas only the stations located in Montsià have been selected for the frequency analysis. This data is complemented with imagery from the Panadella weather radar (Fig. 1), part of the XRAD network ("Xarxa Radars Meteorològics," or Network of Meteorological Radars), and lightning data from the XDD network ("Xarxa Detecció de Descàrregues," or Lightning Detection Network). All three networks are managed by the SMC ("Servei Meteorològic de Catalunya," or Meteorological Service of Catalonia).

Separately, the medium-to-high-level meteorological analysis has been conducted by the National Forecasting Centre of AEMET ("Agencia Estatal de Meteorología," or State Meteorological Agency) using a combination of water vapor channel imagery from the Meteosat-10 and Meteosat-11 satellites (channel 6.2) and outputs from the HRES-IFS model of the ECMWF (European Centre for Medium-Range Weather Forecasts). Additionally, vertical wind profiles and thermodynamic data for the Alcanar area have been obtained from the Harmonie-Arome mesoscale model, also operated by AEMET. Lastly, 3-hourly data from the 5th generation ECMWF global reanalysis ERA5 (Hersbach et al., 2020) has been analyzed to identify the moisture sources fueling the three flood events studied.

The data on flood episodes affecting the Montsià region has been obtained from the INUNGAMA database (initiated by Barnolas and Llasat in 2007) covering the period 1980–2020. Since the database originally ended in 2020, it has been updated to include flood events up to 2023. Regarding damages, they have been estimated using information for the period 1996–2020 from the CCS ("Consorcio de Compensación de Seguros," or Insurance Compensation Consortium), which is ultimately responsible for flood compensations in Spain.

4. Methodology

Given that the primary objective of this article is to enhance the understanding of flood risk in the Montsià region, with a particular focus on the municipality of Alcanar, and to examine the potential influence of climate change on heavy rainfall and flood risk in the area, the article has been structured into three parts. The corresponding methodology for each part is detailed in the following subsections. Fig. 4 shows a diagram of the methodology followed in this paper.

4.1. Characterization and frequency of floods and heavy rainfall in Montsià

The analysis begins with a study of flood frequency and its impacts on Montsià over the period 1996–2023, with particular focus on the municipality of Alcanar due to its high vulnerability. For Alcanar, damage estimates are drawn from CCS flood compensation data spanning 1996–2020, the period for which comprehensive records are fully available. Additionally, the analysis provides an overview of the damages and key aspects of the warning systems and emergency management for the three case studies: October 2018, September 2021, and September 2023.

Flood frequency has been analyzed through the return periods of

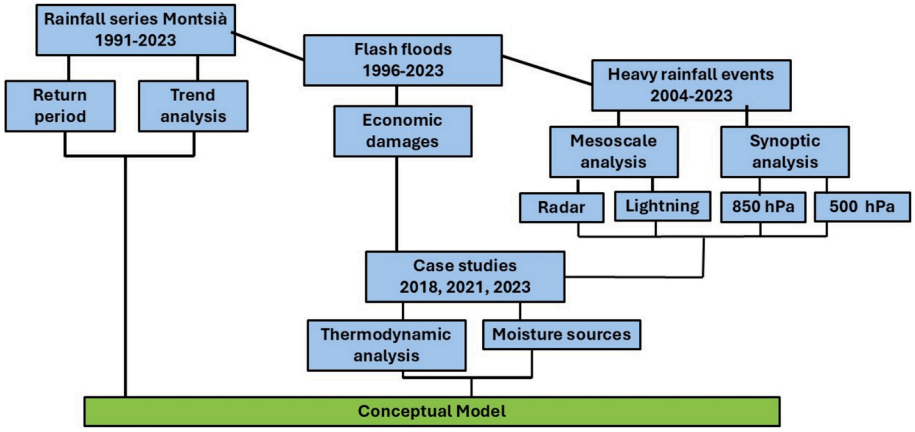

Fig. 4. Schema of the methodology followed in this study.

maximum annual daily and hourly precipitation across various cumulative periods, focusing on six stations in Montsià: Mas de Barberans, Sant Jaume d'Enveja, Alcanar, Amposta, La Ràpita, and Ulldecona (Fig. 3). This analysis has been conducted at both daily and sub-daily scales, with years containing more than 10 % missing data during the period 1991–2023 filtered out to ensure consistency.

Our methodology follows a multi-distributional frequency-analysis framework, specifically adapted for stations with short block-maximum records (around 30 years or less). The approach avoids reliance on a single statistical model by evaluating a range of distributions that represent different theoretical and empirical tail behaviours commonly observed in rainfall data (WMO, 1989; NOAA, 2006). These include the Generalized Extreme Value (GEV) distribution—which encompasses the Gumbel ($\xi = 0$), Fréchet ($\xi > 0$), and reverse-Weibull ($\xi < 0$) types as formal limit laws under extreme value theory, EVT (Coles, 2001; Katz et al., 2002). Additional empirical alternatives, such as the Log-Normal, Gamma, Normal and classical Weibull distributions, are included to capture a wider range of possible distributional shapes, especially when the data are insufficient to reliably constrain the tail behavior through EVT alone.

On this basis, a two-tier selection process is implemented at each station. In the first stage, the Kolmogorov–Smirnov (K-S) test is used to assess the goodness of fit by comparing the empirical and theoretical cumulative distribution functions (Stephens, 1974). Distributions that fail to satisfy the null hypothesis at the 5 % significance level are discarded. In the second stage, the remaining candidates are evaluated using quantile–quantile (Q–Q) plots, with the quantile-based coefficient of determination R^2 calculated to assess how well each model reproduces the observed distribution. This metric is particularly relevant because we aim to provide return levels for a range of recurrence intervals (2, 5, 10, 20, 50, and 100 years), and a good agreement across the entire distribution—including moderate and high quantiles—is essential (Hosking and Wallis, 1997; Papalexiou and Koutsoyiannis, 2013). The model with the highest R^2 is then selected as the best-fitting distribution at each station.

While this methodology provides a consistent and comparative framework for estimating return levels across stations, we emphasize that the use of short records (around 30 years or fewer) introduces substantial uncertainty, particularly for long return periods such as 50 or 100 years. These estimates should therefore be interpreted as indicative of the potential severity that may be attained at a location, not as precise or design-grade thresholds. As such, the approach is well suited for applications in risk awareness and preliminary hazard assessments, but not for hydraulic infrastructure design, where tail-specific fitting methods and longer records are typically required (Koutsoyiannis, 2004).

4.2. Contextualization and analysis of three catastrophic floods: 2018, 2021, 2023

To meteorologically contextualize the flooding episodes of 2018, 2021 and 2023, this analysis begins with a systematic study on all events that exceeded 100 mm/day at any point in the region since 2004, the year when the Panadella radar (Fig. 1) became fully operational. According to Reboita et al. (2024), variations in the storm center are critical for understanding precipitation distribution. For this reason, in the present work, thunderstorm structures have been characterized using both radar and lightning data. Specifically, the storm center and storm top have been derived using the cell-core identification method, which operates in real time at the Meteorological Service of Catalonia and was introduced by Rigo and Llasat (2016). This method is based on threshold criteria initially developed by Rigo and Llasat (2004) and subsequently refined by Del Moral et al. (2018).

To complement this mesoscale analysis, synoptic fields of surface pressure and geopotential height at 850 and 500 hPa have also been examined. These fields—together with those at 700 and 300 hPa—are among the most widely used in studies of convective systems, as they help identify synoptic and mesoscale structures that may favor or inhibit convection. Although such fields do not allow direct inference of the initiation and development of convection, they are essential for assessing whether the broader-scale environment is conducive to convective activity. Numerous studies have demonstrated their usefulness in analyzing convective phenomena over the western Mediterranean (e.g., Ferreira, 2021; Insua-Costa et al., 2021).

Moreover, simulated atmospheric soundings have been extracted at the grid point corresponding to the Alcanar area from the operational Harmonie-Arome limited-area mesoscale model. This has been done following a similar approach to that of Calvo-Sancho et al. (2023). These model-based soundings allow for the estimation of thermodynamic variables in a manner comparable to real observed profiles, thus offering valuable insight into the vertical structure of the atmosphere during the events studied.

Afterwards, it focuses on the three most recent catastrophic flooding events that affected the region: the episodes of 18–19 October 2018, 1 September 2021, and 3 September 2023. It examines precipitation in terms of both its distribution and intensity, as well as the systems that generated it and their evolution. Since all three episodes exceeded 200 mm —occurring within just five years and representing the highest accumulations in the 30-year record— and were remarkable for their highly localized nature, a key question arises: was the source of the precipitated water mass entirely Mediterranean? To address this, the precipitation field over a broader region is analyzed, and the origins of the humidity are traced.

The identification and quantification of moisture sources has been

performed using a Lagrangian moisture tracking methodology. The analysis starts by running the Lagrangian particle dispersion model FLEXPART (Pisso et al., 2019), which divides the atmosphere into individual fluid parcels and tracks them forward in time. FLEXPART has been forced by ERA5 wind fields (along with other variables) and configured to run forward from 30 days before the beginning of each event studied until the end of the event. A global configuration with 15 million air parcels has been employed, of which 9090 are over the area most affected by rainfall during the events (black box in Fig. 5).

Subsequently, using the FLEXPART outputs, we have examined where and how much moisture the parcels arriving in the affected region gained in the days preceding each event, following a similar approach to that of Stohl and James (2004). To isolate only the parcels contributing to the rainfall, we have selected those that lost moisture at the precipitation event (where $dq < 0$ with q representing specific humidity). After identifying the parcels feeding the rainfall, we have determined the areas of specific humidity increase ($dq > 0$) during the previous 30 days, designating them as the source regions.

Additionally, we have applied an end-route moisture discounting procedure, following the method of Sodemann et al. (2008), to exclude moisture uptakes already lost in previous rainfall events. Building on this, we have vertically integrated all remaining moisture uptakes to generate a two-dimensional moisture source field (Fig. 6). This field represents the amount of evaporated water (in mm) from each grid cell that has contributed to the rainfall during the event. Known in the literature as E2P ("evaporation to precipitation"; Keune et al., 2022), it quantifies the contribution of each source region according to the equation below:

$$f = \frac{\sum_{source} E2P}{\sum_{sink} P} \quad (1)$$

Where f represents the fraction of precipitation (P) originating from the source, and the sink refers to the region affected by the event. In Eq. 1, P is derived directly from the ERA5 reanalysis.

The synoptic, mesoscale, and thermodynamic factors responsible for this precipitation are subsequently examined based on the information provided in Section 5.2.

4.3. Trend analysis of floods and extreme precipitation in the region of study

As a third step, we have performed a trend analysis on the six daily and sub-daily precipitation series from the Montsià stations for the period 1991–2023 (Fig. 3). Our methodological framework examines both daily and hourly precipitation datasets, aiming to identify trends across three categories of variables, analyzed on both an annual and seasonal basis -an approach widely used to characterize extremes across multiple temporal scales (Alexander et al., 2006; Blenkinsop et al.,

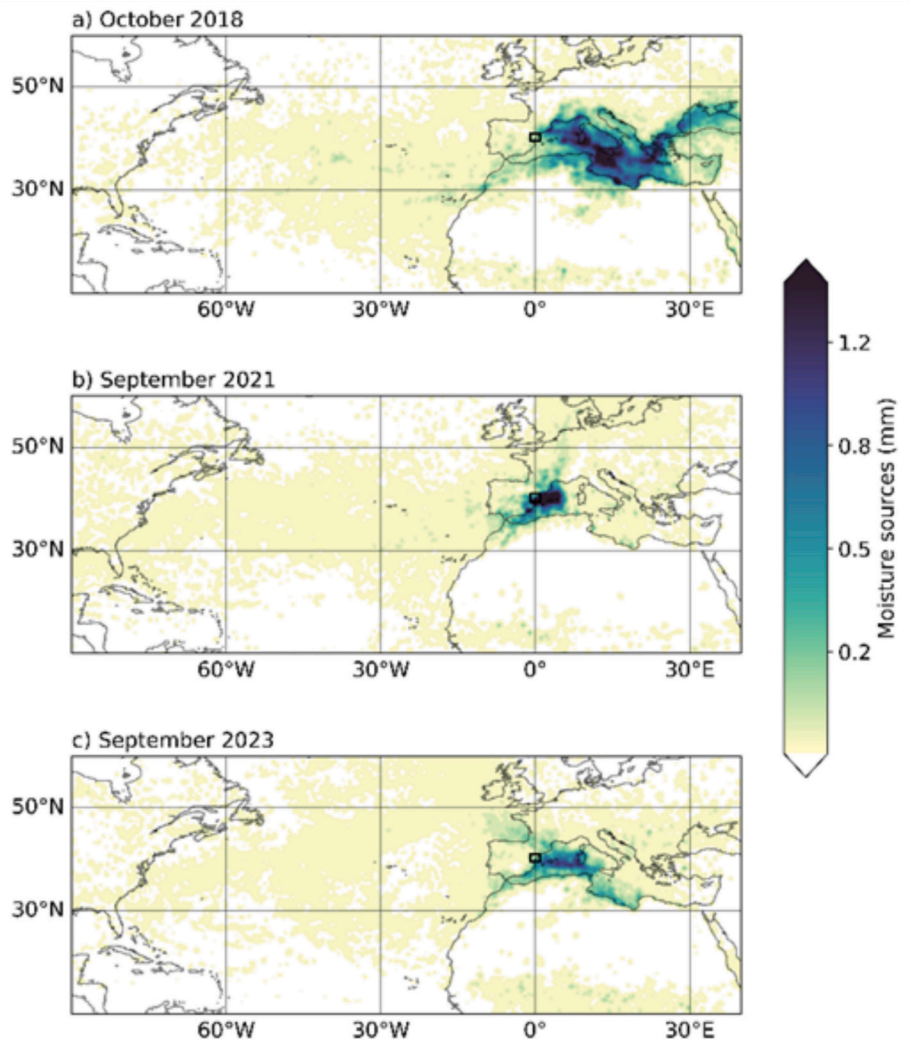

Fig. 5. Moisture source fields (mm) for the October 2018 (a), September 2021 (b), and September 2023 (c) events. The black box highlights the sink region, representing the area affected by extreme precipitation considered in the Lagrangian moisture source analysis.

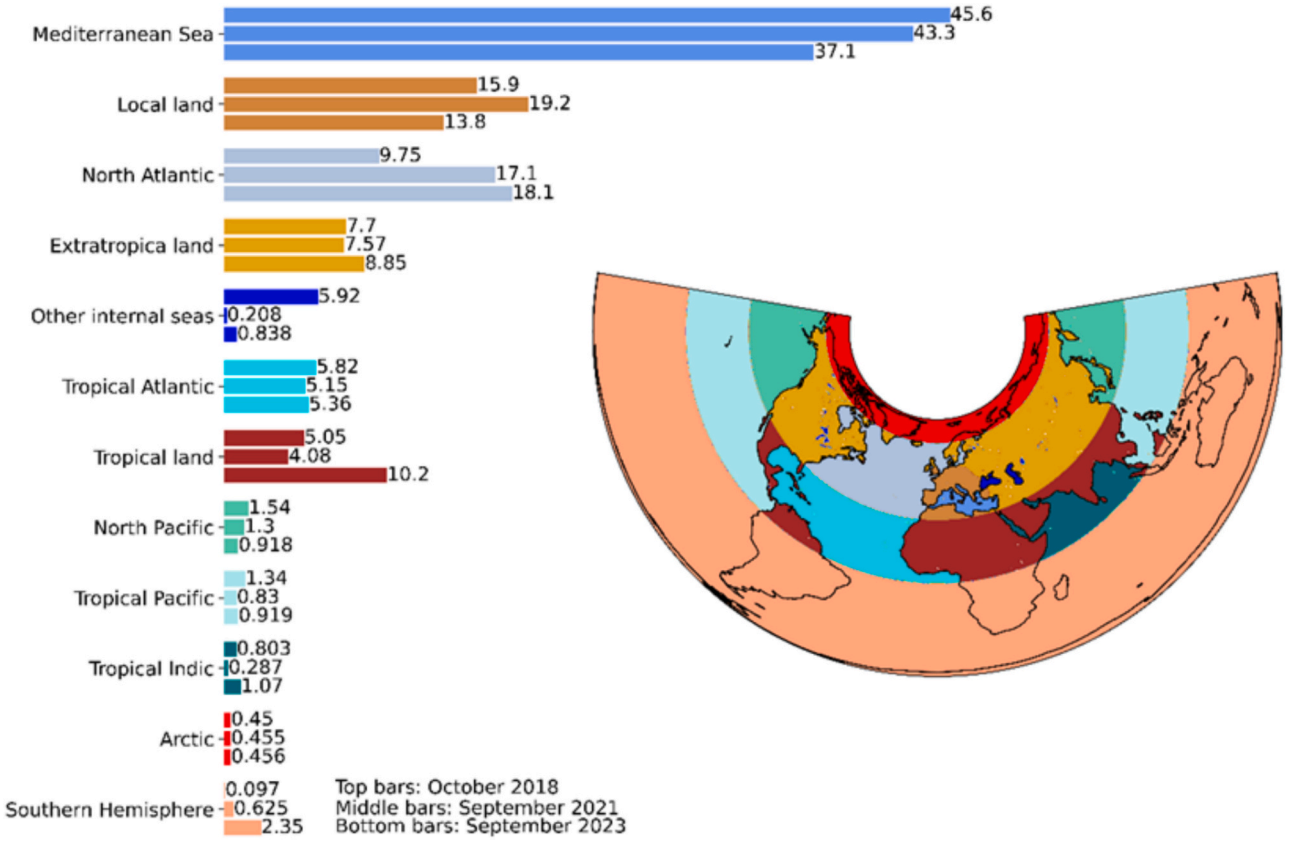

Fig. 6. Precipitation fractions (%) for the October 2018 (top bars), September 2021 (middle bars), and September 2023 (bottom bars) events, categorized by source and represented in different colors in the plot on the right.

2018)—, and identifies trends in three categories of variables, analyzed on both an annual and a seasonal basis:":

1) Variables related to exceeding specific precipitation thresholds. Hourly thresholds of 5, 10, 20, 30, 40, 50, 60 and 90 mm and daily thresholds of 5, 10, 20, 40, 60, 100 and 200 mm span moderate to rare events and are consistent with thresholds employed in previous extreme rainfall studies (Alexander et al., 2006; Westra et al., 2014).

- Evolution of the number of instances (hours or days) in which the thresholds were surpassed.
- Evolution of the precipitation amount falling above those thresholds.

2) Variables describing the statistical distribution of rainfall (after excluding values < 1 mm).

- Trends in the 5th, 50th (median) and 95th percentiles of precipitation.
- Evolution in measures of distribution shape—kurtosis (tailedness), skewness (asymmetry) and variability (standard deviation)—as recommended for comprehensive rainfall diagnostics (Wilks, 2011).

3) Total amount of rainfall.

Trends are quantified using linear regression, with statistical significance evaluated at the 95 % confidence level (Wilks, 2011). The validity of each trend is assessed through a *t*-test on the regression slope, providing a *p*-value. To ensure dataset integrity, years with more than 10 % missing data are excluded, typically resulting in the removal of one to two years per station. Finally, to highlight long-term precipitation patterns and minimize the influence of short-term fluctuations, 5- and 10-year moving averages are applied (Mudelsee, 2010). These averages are visualized alongside the primary data, offering a comprehensive perspective on the overall trends.

5. Results

5.1. Characterization and frequency of floods and heavy rainfall in Montsià region

The updated INUNGAMA flood database records 54 flooding episodes in the Montsià region between 1996 and 2023, 31 of which affected the municipality of Alcanar. This corresponds to an average of about one flood episode per year in Alcanar and nearly two per year across the region. 93 % of these events were flash floods caused by heavy rainfall in Montsià county. In the case of Alcanar, all the events were flash floods. During this period, the monthly distribution of flood episodes in Montsià shows a marked peak in September and November, with 13 episodes each (24 % of the total). As a result, autumn emerges as the season with the highest frequency, accounting for 63 % of all recorded episodes. Of these, 22 episodes exceeded 100 mm of precipitation in 24 h. The remaining 32 episodes did not reach this threshold at monitored stations, though some may have exceeded it elsewhere, as many were characterized by short but highly localized intense rainfall.

Between 1996 and 2020, payments made by the CCS for flood damage have been systematically analyzed using data from the INUNGAMA database. During this period 27 flooding episodes affecting the municipality of Alcanar have accounted for 2,059,655 $€_{2022}$ (adjusted to 2022 values) out of total compensation of 305,339,431 $€_{2022}$ for all of Catalonia, representing just 0.67 % of the total. This relatively modest share reflects the nature of the damage, which has primarily involved homes and second homes, rather than critical infrastructure or industrial areas, which typically generate higher costs. Despite this, the penetration of insured capital in Alcanar during this period is distinctly high,

with average compensation per episode amounting to 76,283 €$_{2022}$.

However, the three case study episodes analyzed in this paper (2018, 2021, and 2023) have greatly exceeded these average compensation values. Fortunately, none of the three cases resulted in fatalities in Montsià. The first case, which occurred from October 18–20, 2018, resulted in CCS costs of 1,416,963 €$_{2022}$, an extraordinary amount 18 times higher than the average. Extending beyond Alcanar, the event incurred total CCS compensation of 3,178,477 €$_{2022}$ across Catalonia, with more than half (1,725,792 €$_{2022}$) concentrated in Montsià county. Despite these large payouts, the total damages from the event were estimated to exceed 8,000,000 €$_{2022}$, underscoring its devastating scale. The flooding also prompted the activation of the INUNCAT emergency plan for Catalonia, with the fire brigades handling more than 50 incidents related to flooding and wind damage. In Alcanar, approximately 80 % of roads were partially or completely submerged, and the FERROCAT railway emergency plan was also triggered as flooded train tracks between northern Valencia and southern Catalonia caused significant disruption to rail services. It is worth noting that two flood events had already occurred in Catalonia earlier that same month, both affecting the Montsià region. The first took place between October 9 and 10, and the second between October 13 and 15. The latter was associated with the approach of Hurricane Leslie to the Iberian Peninsula and also impacted southern France, where it caused the deaths of 15 people.

The flash flood event of September 1, 2021 was among the most severe recorded in Montsià in the last century (Balasch et al., 2023). The heavy, sudden rains on the coast caused several ravines to overflow, while the Sénia River nearly burst its banks in its final stretch. The CCS disbursed 12,494,376 €$_{2022}$, in compensation across Catalonia. Of this mount, 98 % corresponded to Montsià (12,238,476 €$_{2022}$) and in turn 83 % (11,578,501 €$_{2022}$) was allocated to the municipality of Alcanar, which, along with Vinaròs (València), was declared a catastrophic area. Damages were also reported in the neighbouring municipalities of La Ràpita and Ulldecona. This event resulted in payouts that were five times the total CCS compensation for the entire period from 1996 to 2020. The INUNCAT emergency plan was activated on the same day, along with the Special Emergency Plan for Accidental Pollution of Marine Waters in Catalonia (CAMCAT). Several campsites and isolated dwellings had to be fully evacuated, over 200 people were rescued, and 90 % of municipality roads suffered some kind of damage. More than 10,000 homes were left without power, and in the municipality of Alcanar, 600 cars were swept away by the floodwaters. In the seaside village of Les Cases d'Alcanar, the overflow of the Sant Jaume ravine led to water depths reaching 1.5 m in some streets. Key motorways and railways connecting the Spanish Mediterranean coast to France through Montsià were also disrupted. Beyond the physical damage, the floods also had important indirect impacts: several businesses were forced to close for weeks, and fishing activity was suspended for over a week. A psychological support service was deployed by the town council to assist affected residents, while civil society mobilized through the #Monsortirem platform to channel solidarity and raise funds for reconstruction, particularly for those without insurance coverage.

Similarly, in the episode of 3 September 2023, compensation for the whole of Catalonia amounted to 3,973,903 € (3,752,506 €$_{2022}$), with the majority allocated to Montsià and, once again, Alcanar standing out with 1,384,801 € (1,307,650 €$_{2022}$). On this occasion, the INUNCAT plan was also activated, and, for the first time in such events in Catalonia, the Civil Protection mass alert system was employed to send alerts to mobile phones, instructing the confinement of the 9600 residents of the municipality of Alcanar. This marked a significant evolution in emergency response measures, underscoring the efforts to mitigate the potential impacts of such events. In the aftermath, the mayor of Alcanar proposed, for the first time, the possibility of expropriating 50 buildings to create a flood outlet for a ravine in one of the municipality's most affected areas.

Together, these three events represent a turning point in the flood loss record for Alcanar, with compensation amounts far exceeding previous levels. This shift is clearly reflected in the cumulative evolution shown in Fig. 7, where payouts remain relatively low until 2017, followed by a steep increase from 2018 onward. Although the disaster zone was declared in all three flash flood episodes, the episode with the most severe consequences was that of September 2001, which was characterized by rainfall intensities greater than the other two. The INUNCAT plan was activated in all three episodes, but it was in the third that massive telephone alerts were issued. Following this episode, the possibility of expropriating homes located in high-risk areas was raised, as well as seeking nature-based solutions (Sauquet et al., 2023).

To better understand the spatial variability behind these recent high-impact floods, return level analysis of daily precipitation provides insight into localized hazard patterns within Montsià (Fig. 8). These values begin at 112 mm for a 2-year return period and rise progressively to 208 mm for a 10-year period, 300 mm for a 50-year period, and 340 mm for a 100-year period. Within this context, Alcanar emerges as particularly vulnerable to extreme rainfall events, with daily return levels ranging from 67 mm for a 2-year return period to 237 mm for a 50-year period. Likewise, Mas de Barberans, located at the base of the Els Ports Mountain range, shows a pronounced increase in precipitation levels, climbing from 96 mm for a 2-year return period to 310 mm for a 100-year period. By comparison, other Montsià municipalities, including Amposta, La Ràpita, Ulldecona, and Sant Jaume d'Enveja, display a relatively moderate risk profile, reflecting the existing variability within the region.

Building on this analysis, the data in Fig. 9 reveal substantial interannual variability and point to periods where successive years show high return periods. Particularly noteworthy are three events in the past six years in Alcanar, where return periods ranged between 27 and 65 years. By contrast, earlier years seldom saw the annual daily maximum exceed a return period of 7 years. This striking change suggests the potential emergence of a regime shift, with implications for regional hydrological planning and disaster preparedness. The intense hourly rainfall rates for different return periods further emphasize the susceptibility of Montsià to extreme precipitation events. For the region as a whole, these rates range from 45 mm/h for the 2-year return period to 120 mm/h for the 100-year return period. Importantly, the AEMET-defined thresholds for yellow, orange, and red alerts in the study area are 20, 40, and 90 mm/h, respectively. This indicates that, on average, an orange alert for hourly rainfall intensity is expected every two years, while a red alert event is projected slightly more than once every 20 years. Alcanar again stands out, surpassing these thresholds for the 2-, 5-, and 50-year return periods, with a particularly notable deviation from other municipalities starting from the 20-year period.

5.2. Contextualization and analysis of three catastrophic floods: 2018, 2021, 2023

To establish a conceptual meteorological framework, we analyzed episodes exceeding 100 mm of precipitation within 24 h at any of the six meteorological stations in Montsià, spanning the period from 1996 to 2023. Among the 22 identified cases, 36 % occurred within the past five years. The seasonal distribution of these events peaks in autumn, with October being the most significant month, with no such cases recorded in summer. Consequently, these episodes typically occur outside the hottest months, a time when deep convection is more common.

Radar analysis covering 19 cases from 2004 to 2023 reveals a consistent feature across all episodes: the sea-to-shore displacement of precipitation structures. This pattern suggests a substantial moisture input, enhancing the precipitation efficiency. However, the direction of displacement varied significantly, ranging from east to west, southeast to northwest, or south to north. Notably, in 60 % of the cases, the prevailing direction was towards the west or northwest. Beyond the efficiency of precipitation, it is worth noting the phenomenon of recurrence, where rainfall persists over the same location for an extended period. This recurrence can result from either the stationarity of precipitating structures, the so-called convective train effect (repeated passage of

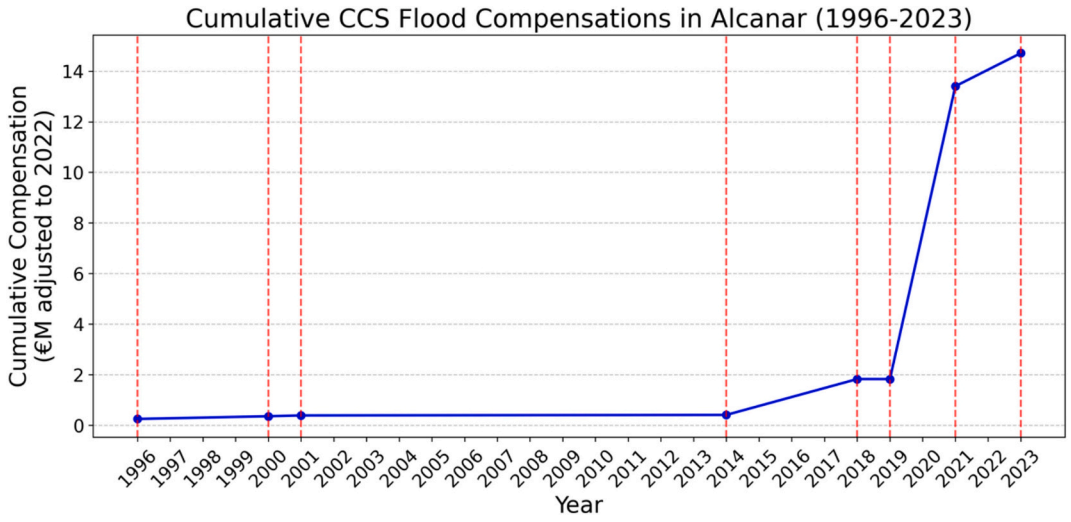

Fig. 7. Evolution of cumulative flood compensations paid by the CCS in the municipality of Alcanar from 1996 to 2023 (€M, adjusted to 2022 values). The vertical red dashed lines indicate episodes for which CCS compensations were paid. (For interpretation of the references to colour in this figure legend, the reader is referred to the web version of this article.)

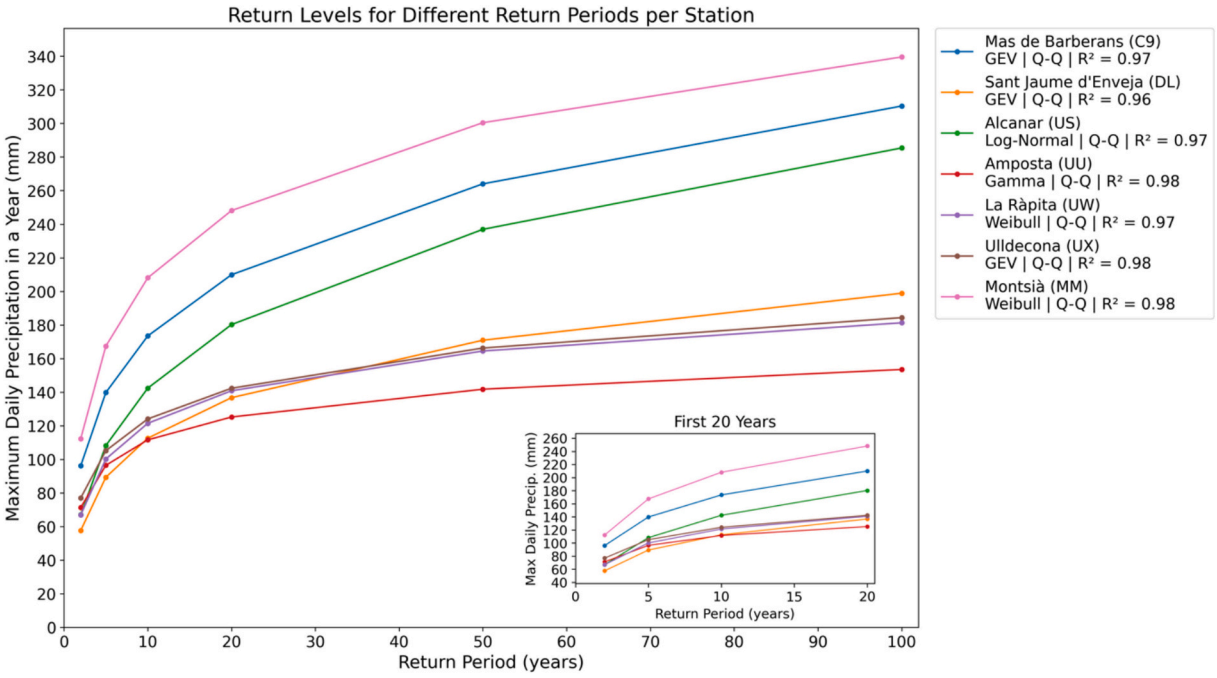

Fig. 8. Adjusted maximum daily precipitation (in mm) as a function of the return period (in years) for each meteorological station and for Montsià county as a whole (code MM). Different statistical distributions, selected based on best fit, are applied for each station, along with their corresponding coefficients of determination for the Quantile-Quantile plots (R^2): Generalized Extreme Value (GEV) for Mas de Barberans (C9, $R^2 = 0.97$), Sant Jaume d'Enveja (DL, $R^2 = 0.96$) and Ulldecona (UX, $R^2 = 0.98$); Log-normal for Alcanar (US, $R^2 = 0.97$); Gamma for Amposta (UU, $R^2 = 0.98$); and Weibull for La Ràpita (UW, $R^2 = 0.97$) and Montsià county (MM, $R^2 = 0.98$). An inset plot highlights the return levels for the first 20 years, providing a clearer view of short-term return periods.

convective cells over the same point), or a combination of both mechanisms. Among the 19 cases with available radar imagery, 53 % exhibited convective trains, 20 % involved embedded convection, and only 13 % were characterized by isolated convection or rain bands. In some cases, these structures may have been part of a Mesoscale Convective System (MCS) extending southward, beyond the coverage area of the Panadella radar.

The degree of organization varied significantly between episodes (Fig. 10). Some events displayed a uniform stratiform precipitation field (Fig. 10a), others featured embedded convection (Fig. 10b), isolated convection (Fig. 10c), or systems with a high degree of convective organization (Fig. 10d). This variability implies that most episodes lasted between 6 and 12 h. More specifically, 40 % of maximum intensities occurred between 12:00 and 18:00 UTC, while 27 % were recorded between 06:00 and 12:00 UTC. Regarding vertical development, 28 % of episodes exceeded 11 km in height, an equal percentage remained below 9 km, and 42 % developed between 9 and 11 km.

Electrical activity in the analyzed episodes is closely associated with the vertical development of precipitating systems. In particular, echo tops exceeding 10 km often appear to be a threshold for lightning initiation. The dataset displays a broad range of lightning activity, from episodes with little or none to those with low or moderate discharges

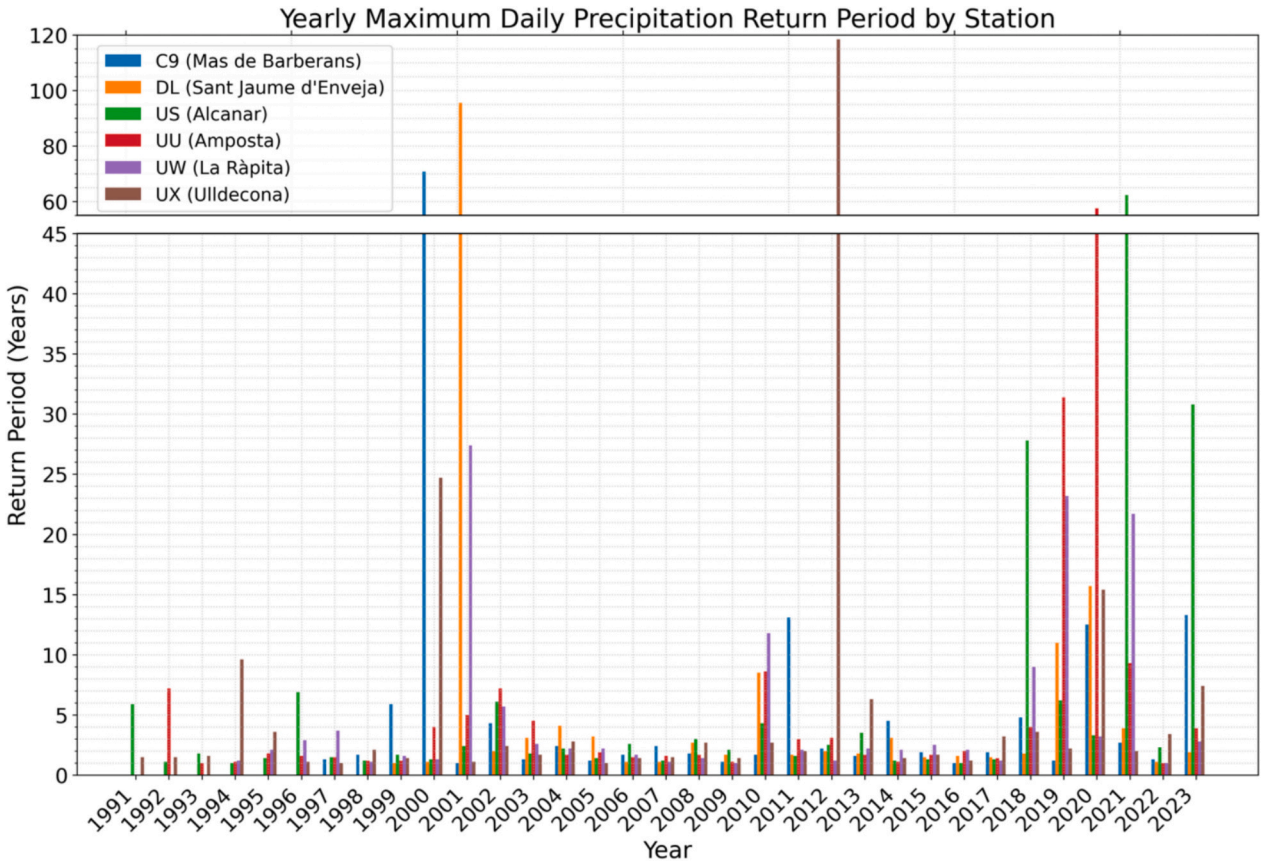

Fig. 9. Return periods (in years) of annual maximum daily precipitation for meteorological stations in Montsià county (1991–2023). Each bar indicates the corresponding return period.

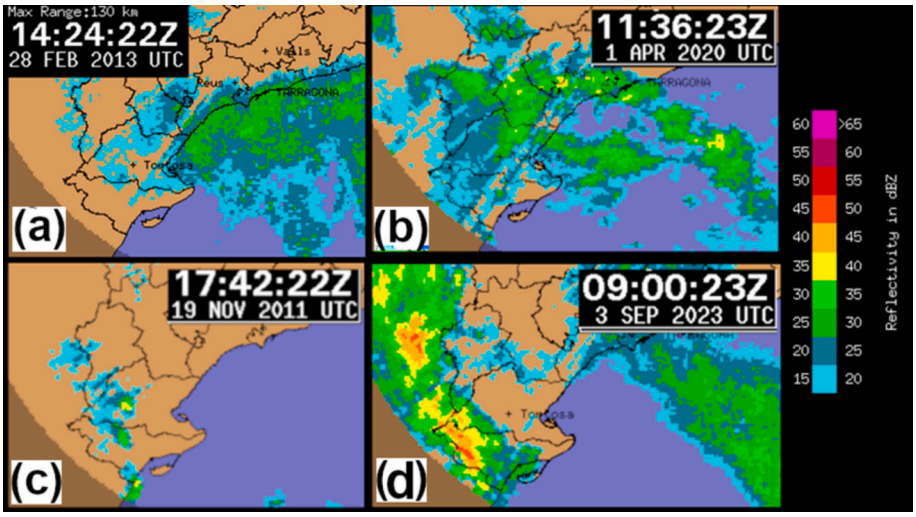

Fig. 10. Examples of precipitation structures during episodes exceeding 100 mm in 24 h in Montsià county: (a) 28 February 2013, stratiform precipitation; (b) 1 April 2020, embedded convection within stratiform precipitation; (c) 19 November 2022, isolated convection; and (d) 3 September 2023, organized convective system.

(only a minority exhibit high electrical activity). Overall, the total number of discharges remains significantly lower than in deep convective systems, where convective cores commonly exceed 15 km in height. Spatially, the sea–land contrast also plays an important role: in most cases, the greatest vertical development, highest reflectivity, and most intense electrical activity are observed offshore. Seasonally, lightning activity peaks in September and October, with somewhat diminished levels in November.

Regarding the synoptic pattern associated with episodes exceeding 100 mm of precipitation, an analysis of the mean fields for these cases confirms the presence of a low-pressure system over the southwestern Iberian Peninsula at 850 hPa. This system produces an easterly flow over Catalonia, extending upward to at least 500 hPa and often associated with a cut-off low, generating a southwesterly component flow at higher

levels (Fig. 11). At the surface, the low-pressure center is frequently located over the Gulf of Cadiz, resulting in a pronounced easterly flow over Catalonia (Fig. 12).

In light of these common synoptic features, the next subsections analyze the three case studies with a focus on mesoscale precipitation structures, convective system behavior, and the spatial distribution of cloud-to-ground electrical discharges.

5.3. Rainfall analysis and precipitation systems

Fig. 13 shows that, in all three cases analyzed, heavy rainfall extended into other regions, leading to flooding in multiple areas. For instance, the episode from October 18–20, 2018, affected not only Catalonia but also Valencia and the Balearic Islands (Fig. 13a). Similarly, the event on September 1, 2021 (Fig. 13b) caused flooding south of Madrid, particularly in Toledo (ARCIMIS, 2021). Although the episode on September 3, 2023, appeared more localized in previous figures, it was actually the tail end of an episode occurring between September 2 and 4, which affected substantial areas of the Iberian Peninsula and caused severe flooding also in Toledo and the Community of Madrid (Fig. 13c).

5.3.1. Rainfall analysis and precipitation systems: 18–20 October 2018 event

During the catastrophic flooding event of October 18–20, 2018, in Catalonia, the most intense rainfall, with daily accumulations exceeding 100 mm (Fig. 14a), began after 12:00 UTC on the 19th in Baix Ebre and Montsià counties. The maximum recorded rainfall for this day was 209.6 mm in Els Ports. On the same date, Alcanar recorded 199.8 mm, concentrated over a six-hour period (12:00–18:00 UTC), with a peak 30-min rainfall of 52.4 mm around 15:30 UTC. Overall, between October 18 and 19, much of Montsià and Baix Ebre received more than 150 mm of precipitation, with a maximum of 312.2 mm in Els Ports de Tortosa-Beseit and 266 mm in Alcanar.

From a radar perspective, the precipitation structures during the October event moved from E-SE to W-NW, exhibiting a linear organization of convective cells that formed a convective train. This train remained nearly stationary over the area of interest for most of the time precipitation occurred in Alcanar. Fig. 14b illustrates this convective train during the period of highest rainfall intensity. Notably, the general structure moved almost perpendicularly to the coastline, gradually shifting from the central Catalan coast towards the Ebro Delta. This pattern aligns with the conceptual model of Doswell et al. (1996), confirming the combination of two simultaneous movements: the general structure's motion from SW to NE and the internal movement of convective cells from SE to NW, which contributed to the system's stationarity.

As shown in Fig. 14c, the storms developed over the sea, with maximum reflectivity values around 55 dBZ. However, their vertical development was relatively modest, not exceeding 12 km at their highest points. Throughout the episode, the storm cores only reached altitudes between 1 and 4 km. The maximum rainfall intensity coincided with the maximum development of the core, which extended around 4 km between 13:00 and 18:00 UTC. These observations are supported by the daily maximum echotop (i.e., the maximum height reached by the cloud as detected by radar) of 12 dBZ, depicted in Fig. 13c. The echotop data indicate that vertical developments rarely surpassed 13 km, predominantly over the sea. Consequently, most lightning activity occurred over the Mediterranean, while lightning over the coast was concentrated primarily in the Alcanar area and its surroundings.

5.3.2. Rainfall analysis and precipitation systems: 1 September 2021 event

Although rainfall was widespread across Catalonia on September 1, 2021 (Fig. 15a), heavy precipitation was concentrated in the southern region, particularly in Baix Ebre and Montsià, where Alcanar recorded a maximum of 251.9 mm within 24 h. Most of this accumulation occurred in just over three hours, primarily between 09:00 and 12:00 UTC, with a 30-min peak of 72 mm and four additional periods exceeding 20 mm in 30 min. Beyond the flash floods, the heaviest rainfall occurred downstream of the River Sénia reservoir, in areas where reservoir regulation offered no flood mitigation potential. The event also reshaped the coastal landscape: the force of the runoff transported large volumes of sediment along the lower River Sénia, which accumulated at the river's outlet—previously obstructed by a gravelly beach ridge—forming a tongue-shaped deposit in a protected coastal area of high ecological value.

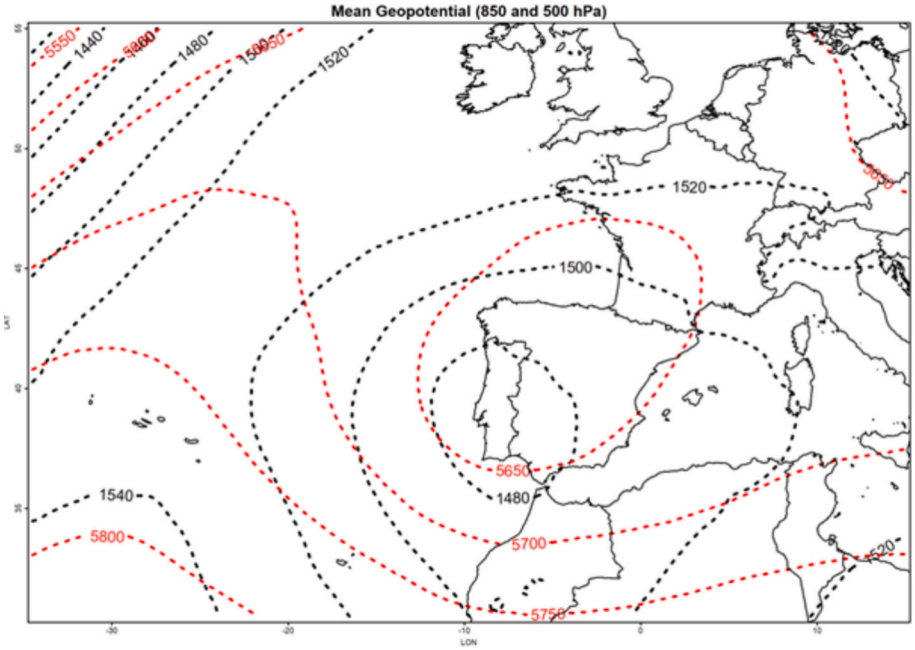

Fig. 11. Daily averaged geopotential height fields at 500 hPa (red contours) and 850 hPa (black contours), derived from ECMWF outputs, corresponding to days exceeding 100 mm precipitation in Montsià county during the 2004–2023 period. (For interpretation of the references to colour in this figure legend, the reader is referred to the web version of this article.)

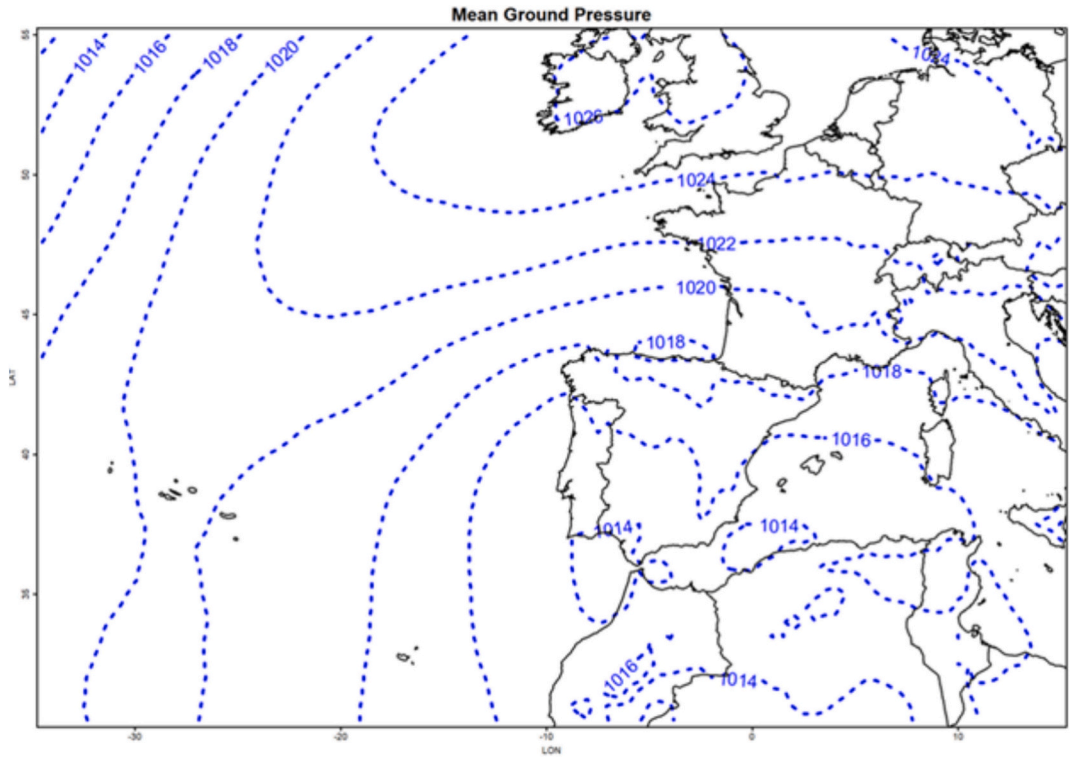

Fig. 12. Daily averaged sea-level pressure fields derived from ECMWF outputs corresponding to days exceeding 100 mm of precipitation in Montsià county during the 2004–2023 period.

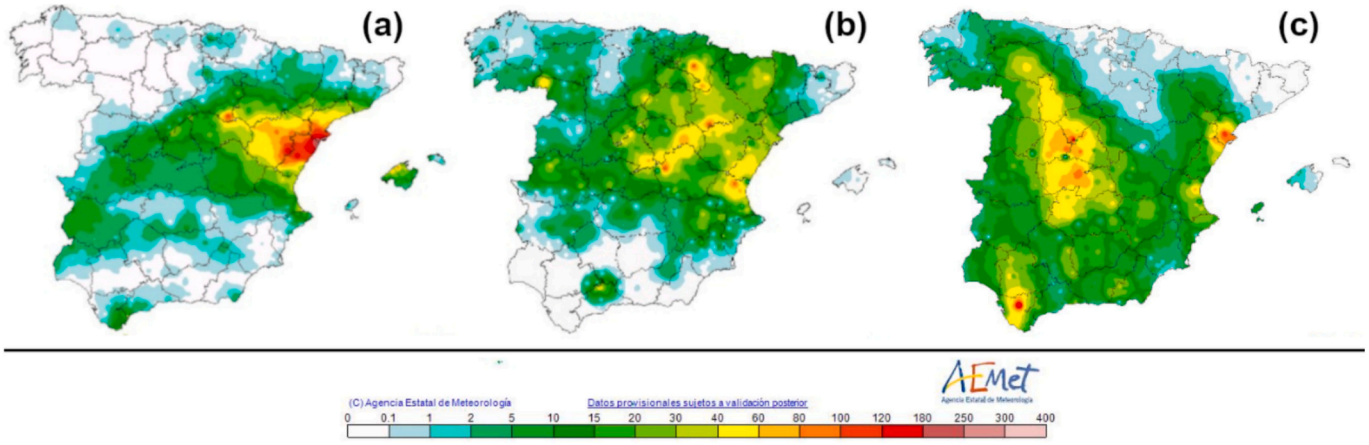

Fig. 13. Precipitation distribution over Peninsular Spain and the Balearic Islands on: (a) 19 October 2018, (b) 1 September 2021, and (c) 3 September 2023. Source: AEMET.

This case stands out from the other two in terms of the evolution of radar structures, as no clear clustering of storms was observed, and the reflectivity field was more fragmented. In this instance, storms moved parallel to the coastline, originating from the south. Just before reaching the Delta area, they developed to a greater vertical extent, discharging over Alcanar municipality before returning to the sea and dissipating rapidly. These dissipating cells acted as triggers for new convective structures, which developed over the remnants of the previous cells. The coastal mountain range further contributed to convection initiation while promoting the system's stationarity. Although reflectivity values were less intense compared to the previous case, the vertical development over the area of interest was higher, reaching 15 km (Fig. 15b). The core tops were at 6 km in maximum height between 9.00 and 15.00 UTC, with the center altitude close to 3 km. The daily maximum height map of the 12 dBZ echotop (Fig. 15c) reveals maxima concentrated over the Alcanar sector, accompanied by strong electrical activity. While most lightning strikes occurred over the sea, a noteworthy maximum coincided with the area where precipitation exceeded 50 mm within 24 h.

5.3.3. *Rainfall analysis and precipitation systems: 3 September 2023 event*

On September 3, 2023, very heavy rainfall was recorded once again in Montsià. However, this episode was apparently more localized than the two previous events, affecting only southern Catalonia (Fig. 16a). Two daily maximum rainfall cores were observed: one north of the Delta and another in Alcanar, where a maximum rainfall of 206 mm/24 h was recorded. Nearly all of this precipitation occurred during the early morning hours, between 04:30 and 07:00 UTC. During this period, the 30-min alert threshold was exceeded in every half-hour interval, with a

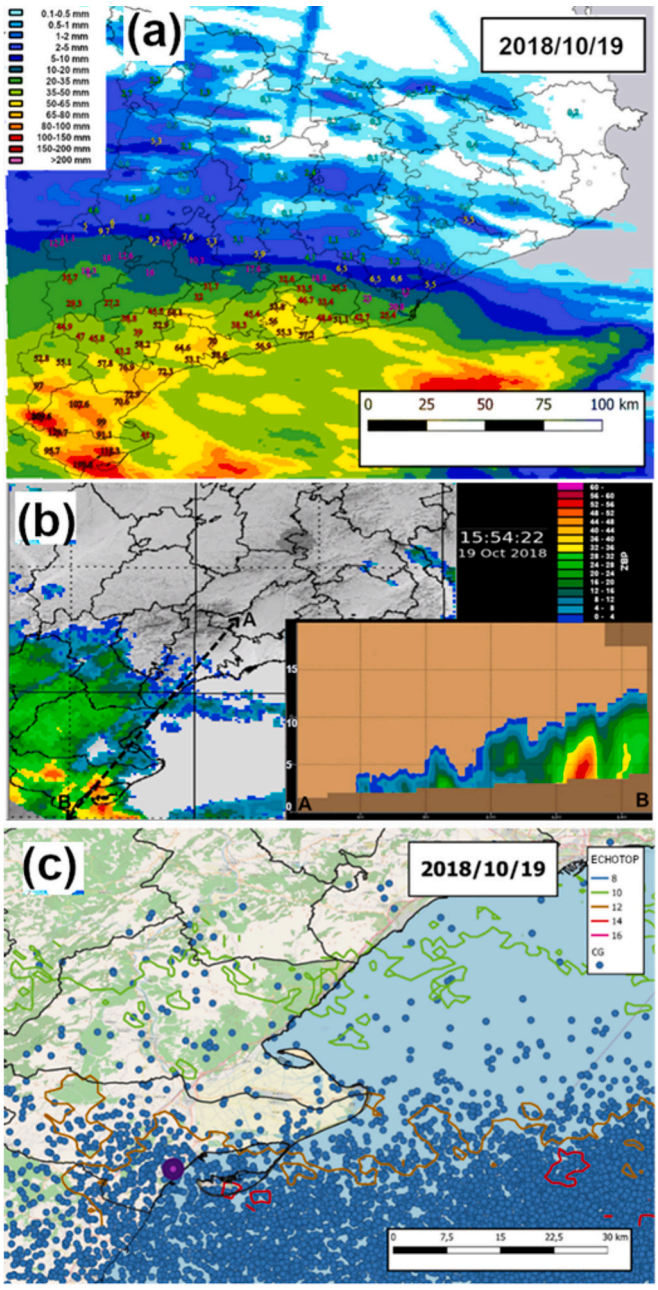

Fig. 14. 19 October 2018: (a) Daily rainfall field estimated from the combination of rain gauge and radar data, showing the locations of XEMA stations; (b) radar reflectivity (dBZ) from CAPPI-4 km at 15:54 UTC, including the vertical section between points A and B; (c) cloud-to-ground electrical discharges and maximum echotop-12 dBZ height (km). Data source: SMC.

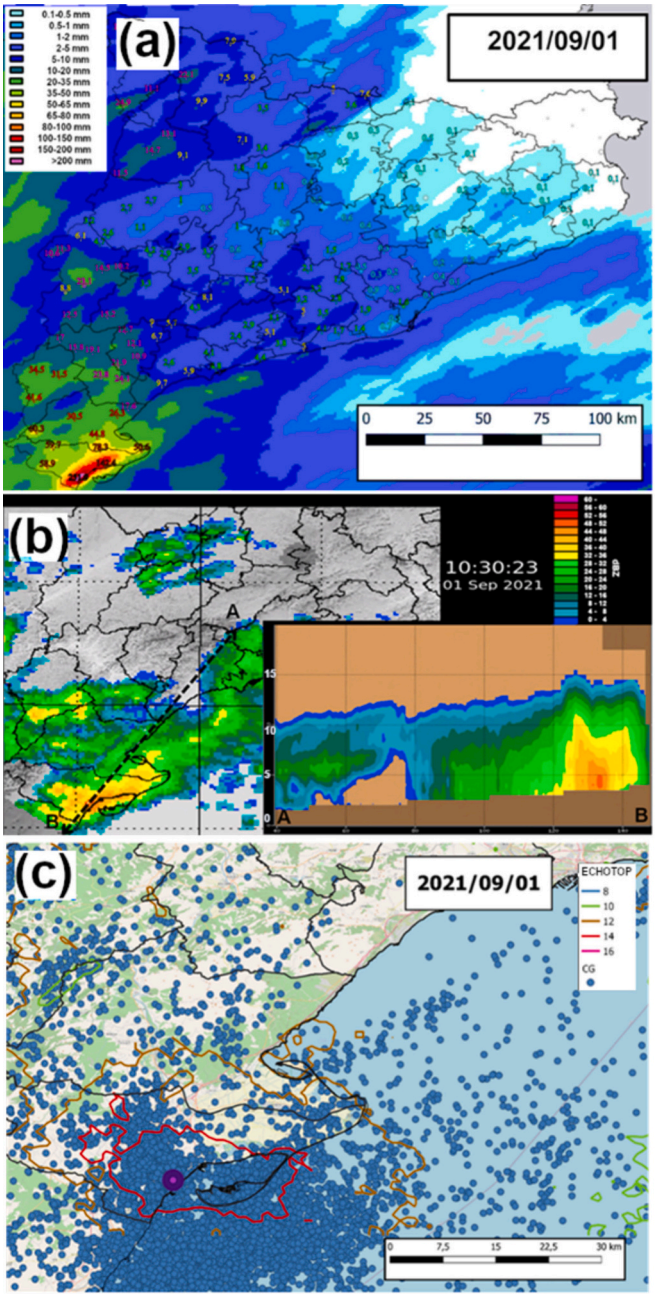

Fig. 15. 1 September 2021: (a) Daily rainfall field estimated from the combination of rain gauge and radar data, showing the locations of XEMA stations; (b) radar reflectivity (dBZ) from CAPPI-4 km at 10:30 UTC, including the vertical section between points A and B; (c) cloud-to-ground electrical discharges and maximum echotop-12 dBZ height (km). Data source: SMC.

peak of 61.4 mm/30 min. This suggests a more intense and concentrated event in both time and space compared to the two prior episodes in the Spanish Mediterranean area.

The spatial distribution of daily precipitation reveals the entry of convective cells from the sea, following a SE-NW trajectory. This movement is reflected in the evolution of the radar field, which, as in the 2018 episode, was characterized by the displacement of the precipitation system parallel to the coastline and the propagation of convective cells from sea to land. In this case, reflectivity values were comparable to those of the 2021 episode, indicating less intense precipitation (Fig. 16b). However, the structures exhibited greater vertical development, reaching heights of up to 15 km. Unlike the previous episodes, the high intensities were sustained for a longer duration, possibly due to the continued presence of storm cells over the same area.

Compared to the earlier events, the 12 dBZ echotop field resembled that of the 2021 episode, while the electrical activity—concentrated again in the Alcanar area—was lower than in the two previous cases (Fig. 16c). The maxima tops and the storm-center had altitudes between 5 and 6 km and 2.5 km, respectively, between 00.00 and 10.00 UTC. This episode can be characterized as highly efficient in terms of rainfall but less severe in terms of storm intensity.

5.4. Synoptic context

The synoptic environment of the three events was defined by the presence of an isolated high-altitude depression, known in Spanish as

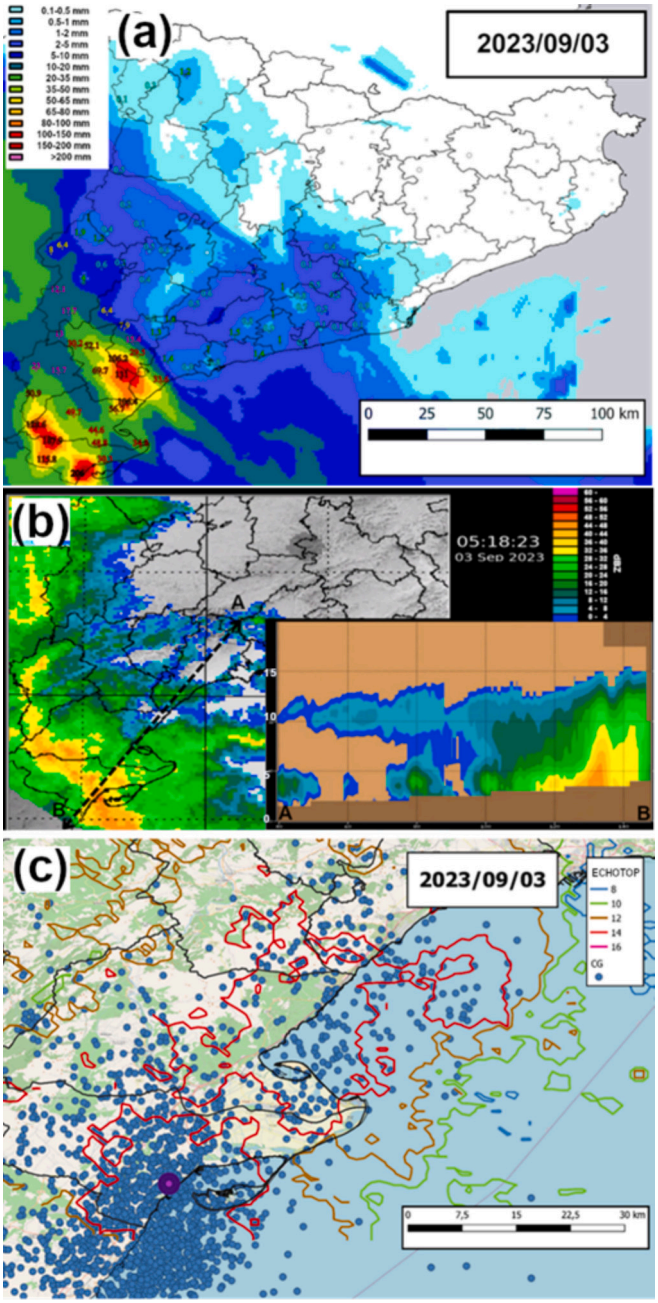

Fig. 16. 3 September 2023: (a) Daily rainfall field estimated from the combination of rain gauge and radar data, showing the locations of XEMA stations; (b) radar reflectivity (dBZ) from CAPPI-4 km at 05:18 UTC, including the vertical section between points A and B; (c) cloud-to-ground electrical discharges and maximum echotop-12 dBZ height (km). Data source: SMC.

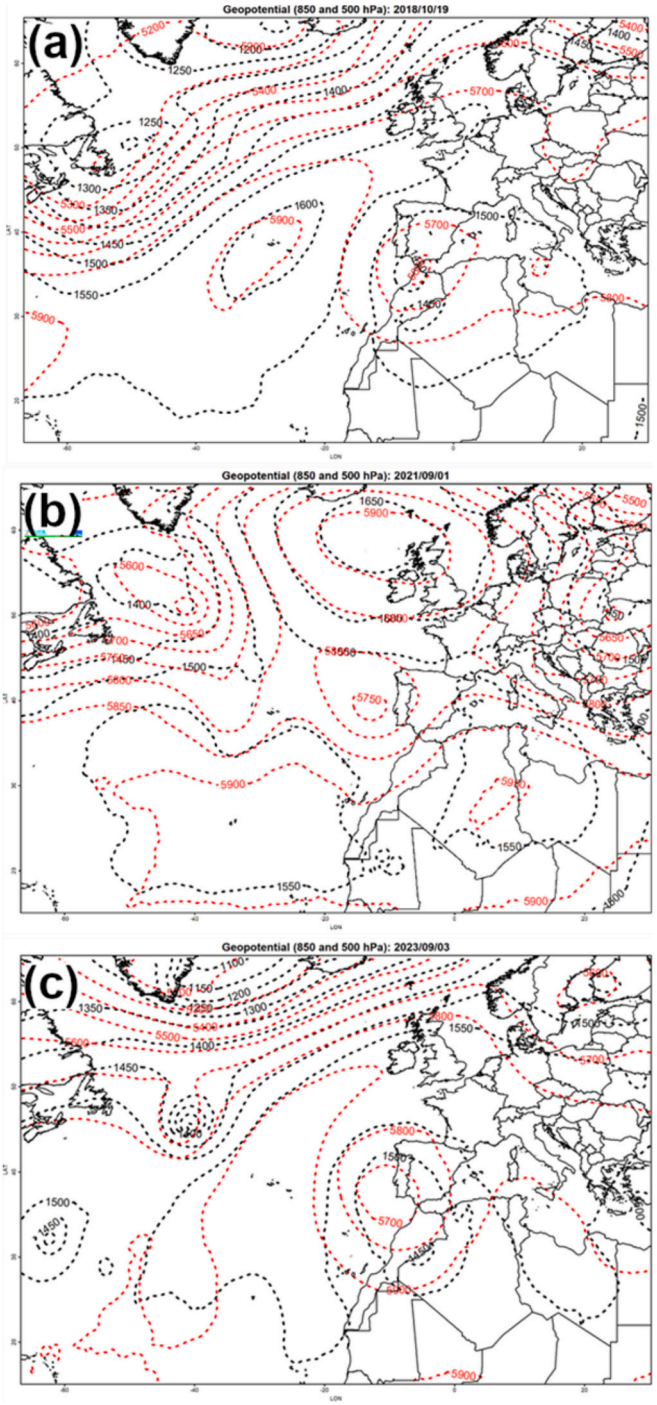

Fig. 17. Geopotential height (m) at 500 hPa (red contours) and 850 hPa (black contours) from ECMWF outputs at 00:00 UTC for (a) 19 October 2018, (b) 1 September 2021, and (c) 3 September 2023. The maps are plotted at 00:00 UTC for comparison with the situations described in Section 5.1. (For interpretation of the references to colour in this figure legend, the reader is referred to the web version of this article.)

"DANA" ("Depresión Aislada en Niveles Altos" or isolated depression at high levels) or "COL" (cut-off low), with a cold core at its center, exhibiting temperatures between −14 °C and − 18 °C at 500 hPa in the vicinity of the Iberian Peninsula (Fig. 17). In the 500 hPa analyses from the HRES-IFS model of the ECMWF, corresponding to the hour closest to the maximum rainfall intensity, the COL centers were respectively situated between the Strait of Gibraltar, San Vincente Cape (Fig. 1), and the southern coast of Portugal. In all cases, the study area was positioned in the northeast quadrant of the COL's area of influence. This region is characterized by synoptic-scale forcing conducive to deep convective developments, with diffluent flow at 500 hPa and temperatures at that level ranging from −9 °C to −14 °C, depending on the event. However, the depth and spatial extent of the COLs varied across the cases. The COL on 1 September 2021 was the least defined (not detected at 850 hPa; see Fig. 17b), while the one on 3 September 2023 was the most pronounced and deepest (Fig. 17c).

The surface and frontal pressure analysis for the hours closest to the events (Fig. 18) revealed distinct characteristics, although a shared feature in all three cases was the synoptic easterly flow of weak to moderate intensity affecting the entire Iberian Peninsula. In the cases of

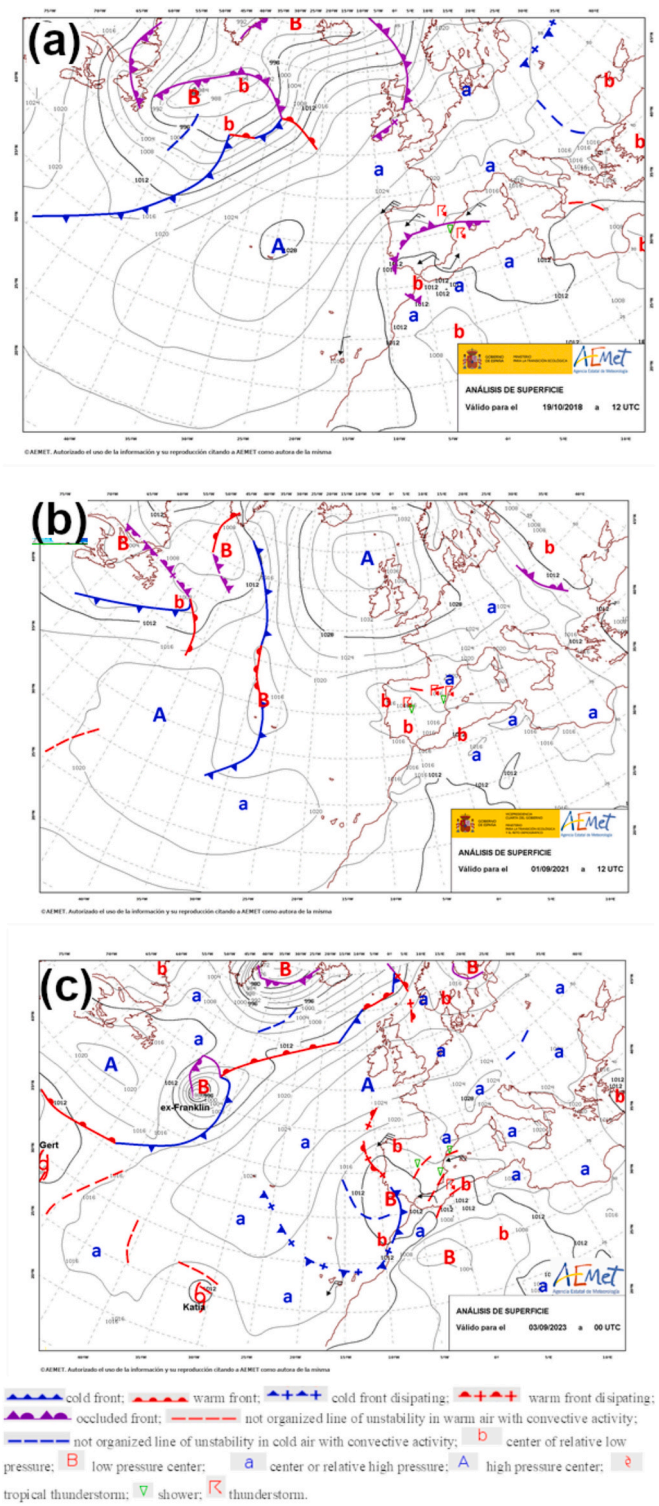

Fig. 18. Surface analysis at: (a) 12 UTC on 19 October 2018, (b) 12 UTC on 1 September 2021, and (c) 00 UTC on 3 September 2023. Source: AEMET.

19 October 2018 (Fig. 18a) and 1 September 2021 (Fig. 18b), there was only a poorly defined area of relative low pressure over the southern Iberian Peninsula and North Africa. By contrast, the episode on 3 September 2023 (Fig. 18c) featured a well-formed low-pressure system of 1010 hPa, centered at 00 UTC over San Vicente Cape. This suggests that the synoptic situation on 3 September should be classified not as a COL, but rather as a cold low—an unusual configuration for this geographical area and time of year. Furthermore, during the event on 1 September 2021, a powerful anticyclone (1038 hPa) northwest of Scotland extended a secondary ridge towards Catalonia in the north-eastern Iberian Peninsula. This played a critical role in establishing the easterly flow over the peninsula and the study area. In the other two cases, an Atlantic-European anticyclone also contributed to the Mediterranean-origin synoptic surface flow, albeit with less influence than in the 2021 episode.

Fig. 19 presents the diagnostics for the time period closest to the peak intensity of the episode in Montsià. The medium- to high-level diagnostics highlight additional sub-synoptic elements that may have contributed to the development of deep convection and the associated heavy rainfall. Notably, jet streaks near the study area can be identified. For the 19 October 2018 (Fig. 19a) and 1 September 2021 (Fig. 19b) cases, a wind maximum was located such that its outflow was positioned to the left of the deep convective activity impacting the Alcanar area. According to the four-quadrant model (Uccellini and Johnson, 1979),

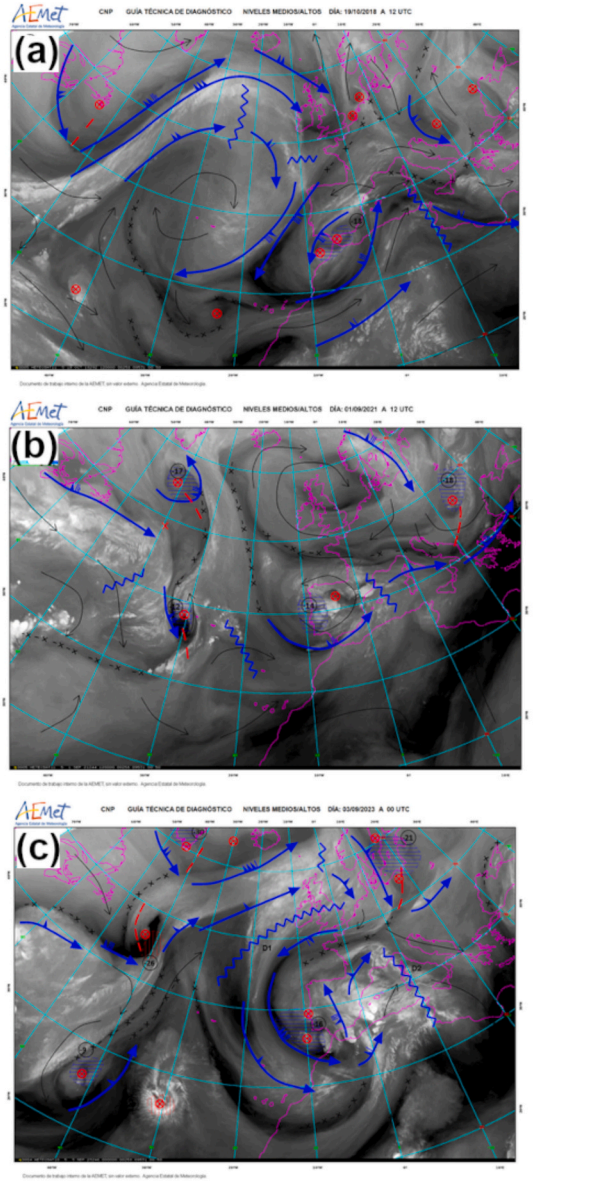

Fig. 19. Diagnosis at mid-upper levels at: (a) 12 UTC on 19 October 2018, (b) 12 UTC on 1 September 2021, and (c) 00 UTC on 3 September 2023. Source: AEMET.

this is one of the regions around a jet stream where conditions are favorable for deep convection. In contrast, the event on 3 September 2023 (Fig. 19c) showed a more intricate arrangement of wind maxima, making direct application of this conceptual model less straightforward. During this episode, a jet stream formed on 1 September to the west of the British Isles, reaching an intensity of 100 knots and aligning southward along the boundary between a North Atlantic ridge and a broad trough with its axis over the British Isles and western Iberian Peninsula. By 2 September, the COL had formed, and the associated vorticity caused the jet stream to split into two branches: one heading south along the western Iberian Peninsula, exceeding 120 knots, and another weaker branch directed northward along the eastern side of the peninsula. This configuration facilitated the eastward growth of the COL, positioning Montsià to the left of the eastern branch by 3 September (AEMET, 2023).

5.5. Mesoscale and thermodynamic analysis

The analysis of vertical wind profiles for the Alcanar area (Fig. 20), derived from the Harmonie-Arome limited-area mesoscale model, reveals that the flow was easterly or south-easterly up to at least 850 hPa on 1 September 2021 (Fig. 20b). In contrast, in the other cases, this easterly or south-easterly flow extended to much higher altitudes: reaching 500 hPa on 3 September 2023 (Fig. 20c) and nearly the upper limit of the troposphere (300 hPa) on 19 October 2018 (Fig. 20a).

Above this E/SE flow, the 1 September 2021 and 3 September 2023 cases exhibited a south or south-westerly flow, consistent with the presence of the COL. This configuration generated vertical wind shear, a condition that can favor the organization of convection once it is initiated. The thickness of the maritime flow ensured that the atmosphere was humid or very humid across much of the lower and middle troposphere, extending to 300 hPa in the case of 19 October 2018. This resulted in high precipitable water (PW) content in the atmospheric column over the area, one of the key ingredients for the occurrence of heavy or abundant precipitation (Doswell et al., 1996). The maximum PW values in the column (from the surface to 300 hPa), extracted from soundings for the area, ranged between 33.3 mm and 54.1 mm. However, values exceeding 40 mm were prevalent at locations such as Alcanar, La Sénia, and Amposta, with no significant differences observed between these points.

The analysis of atmospheric stability during the period closest to the intense rainfall (Fig. 15), based on the CAPE (Convective Available Potential Energy) index (Moncrieff and Miller, 1976), yields inconclusive results. CAPE values at the time of the episodes ranged from a very low 33 J/kg on 19 October 2018 to moderate levels of 623 J/kg on 1 September 2021 and 826 J/kg on 3 September 2023. Notably, in the 19 October 2018 case, the CIN (Convective Inhibition) index (Colby, 1984) reached 66 J/kg, exceeding the CAPE value and potentially limiting convection.

However, it is important to note that CAPE values can fluctuate significantly throughout the day due to differential advections of temperature and humidity, which modify the vertical profiles. For instance, at 00 UTC on 19 October 2018, the CAPE was 116 J/kg, four times higher than the value observed 12 h later. Similarly, on 1 September 2021, the CAPE at 00 UTC was 2033 J/kg, more than double the value recorded at 12 UTC, the time closest to the rainfall episode.

Thus, these three convective episodes occurred in environments with limited instability in middle levels, likely due to their distance from the cold core of the COL. This modest instability may explain why deep convection remained isolated in the northeastern Iberian Peninsula. However, where it did occur, convection was highly efficient due to the abundant atmospheric humidity. As previously discussed, the overlap of jet streaks with local maxima in precipitable water (PW) likely played a critical role in focusing and enhancing the convective processes in these areas.

In addition to the CAPE analysis, the Equivalent Potential Temperature (EPT) values at low levels (within the first 50 hPa) were examined,

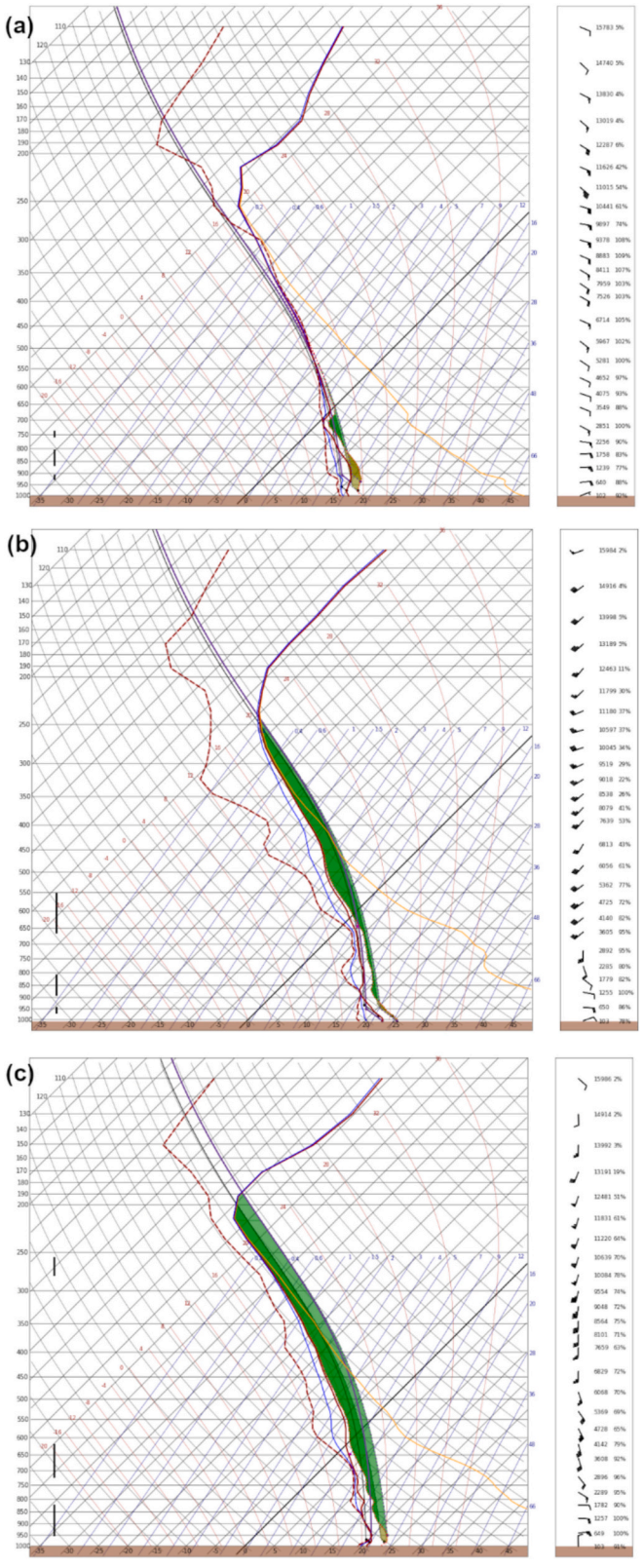

Fig. 20. Soundings from the Harmonie-Arome limited-area mesoscale model analysis over Alcanar, taken at the closest hour to the intense rainfall in Montsià: (a) 12 UTC on 19 October 2018, (b) 12 UTC on 1 September 2021, and (c) 00 UTC on 3 September 2023.

revealing consistently high values across all three episodes, ranging from 40 to 65 °C, with most values exceeding 45 °C. These elevated EPT values highlight the significant role of humidity in the lower atmospheric layers in contributing to potential instability and the possible development of convection. This underscores the importance of humidity content in these episodes, especially since the CAPE values were not particularly remarkable.

5.6. Analysis of the sources of humidity

Fig. 4 shows the moisture source fields for the three events. The first thing standing out from this figure is that the main source of moisture is the Mediterranean Sea in all the cases, but with important differences among them. While for the October 2018 event the Mediterranean moisture contribution was more distributed over the whole basin, even with maximum values in the Central Mediterranean, in the September 2021 case the moisture contribution was restricted to the Western Mediterranean and especially near the coast, just offshore of the affected area. For the September 2023 event, the contribution from the Western Mediterranean was also dominant but with significant moisture uptakes over the central part of the basin.

These differences are linked to the varying synoptic configurations, specifically the positioning of the anticyclone to the north of the Iberian Peninsula and the low-pressure system over North Africa, which shaped the atmospheric dynamics in each case. In October 2018, the synoptic setup favored a long-track easterly flow, enabling moisture transport from as far as the Black Sea, as seen in Fig. 4a. This prolonged flow likely resulted in the air mass becoming saturated before reaching the westernmost Mediterranean, thereby explaining the relatively low moisture uptake in that area. In September 2021, however, the easterly flow was weaker, and moisture convergence from nearby regions became the predominant source. Finally, the September 2023 event represented an intermediate scenario, with characteristics between the two preceding cases. Additionally, Fig. 5 reveals minor moisture uptakes from a range of secondary sources, including nearby landmasses, the North Atlantic, and even tropical regions of Africa.

A quantitative analysis in terms of precipitation fractions (Eq. 1) provides further insight into the relative importance of the different moisture sources (Fig. 6). Indeed, the Mediterranean Sea was the main source in all cases, contributing approximately 40 % of the total moisture, with the highest values observed in October 2018. Nonetheless, five additional sources (according to our definition), also played critical roles in explaining the significant rainfall accumulations recorded. Local land areas and the North Atlantic Ocean consistently ranked as the second and third most important sources in all three events, with contributions ranging between 10 % and 20 %. As an example, contributions from the North Atlantic were significantly larger in the September 2021 and 2023 cases (~20 %) compared to the October 2018 case (~10 %), primarily due to the previously mentioned strong easterly flow in the latter. More remote continental areas also had significant contributions (~8 %) in all three cases, which based on Fig. 5 would come mainly from evaporation over North America. The Black Sea, while relatively minor overall, played a noteworthy role in the October 2018 event (~6 %), but its influence was negligible in the other two cases. Similarly, tropical regions, particularly the tropical Atlantic and Africa, contributed meaningfully to all extreme events. For example, in the September 2023 event, their combined contribution exceeded 15 %. Lastly, when all continental sources are combined, they account for approximately 30 % of the total moisture in each case. This substantial contribution is consistent with expectations for September, when evapotranspiration over land remains a significant source of atmospheric moisture.

Fig. 21 shows a conceptual model that tries to synthetize all the results previously discussed. At the synoptic scale, it shows a surface anticyclone over northern Europe that promotes the stationarity of the disturbance and sustains an east-northeast flow capable of advecting moisture from forested continental regions. It also depicts a DANA (or COL) in the Gulf of Cádiz, which in some cases is reflected at the surface, as a deep low-pressure system. In both cases, it induces a south westerly upper-level flow over the eastern part of the Iberian Peninsula, advecting moist air from the Atlantic. At the mesoscale, there is a distinct advection of warm, humid air from the Mediterranean at low levels, favored by a depression that forms on the leeward side of the Atlas Mountains. Simultaneously, in the affected area a line of instability often develops, sometimes in association with a passing warm front. Finally, at the local scale, elevated sea surface temperatures (SSTs) in the southern part of the Ebro Delta favor moisture feedback, while the surrounding mountainous terrain enhances upward motion through orographic lifting. The diagram is completed by illustrating the vertical structure of the precipitation system and storm activity in relation to the orography.

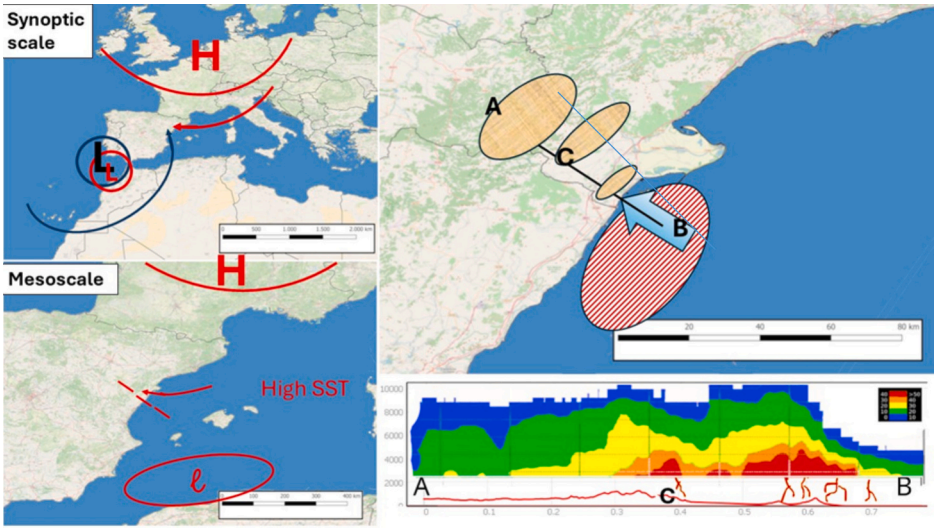

Fig. 21. Conceptual model summarizing the factors associated with heavy rainfall events in the Montsià region. Mesoscale and synoptic scale: blue colour: 500 hPa, red colour: surface; the arrows indicate the main streamlines and the water vapor advection; instability line (discontinuous). Local scale: main trajectory of the convective systems from B to A and mountain systems (brown ellipse); area with the highest SST (dashed area in red); vertical structure of echo radar of the precipitation systems in the mature phase (blue: 0–10 dBz, red:>40 dBz) showing the orography line and the main electric activity inland. (For interpretation of the references to colour in this figure legend, the reader is referred to the web version of this article.)

5.7. Trend analysis

The analysis of flooding trends in Alcanar for the period 1991–2023 suggests a slight upward trend, with an increase of approximately 0.4 events per decade, statistically significant at the 95 % confidence level based on the Mann-Kendall test. At the Montsià level, a positive trend of similar magnitude is observed, but it does not reach statistical significance. A detailed examination of hourly and daily precipitation patterns in the Montsià region offers valuable insights into local climate variability and dynamics. The range of observed behaviours underscores the importance of applying multiple analytical approaches to identify these changes effectively. In this study, precipitation percentiles, exceedance thresholds, and variability metrics—including kurtosis, skewness, and standard deviation—were used to comprehensively characterize precipitation trends in the region.

Precipitation percentiles offer a first indication of how rainfall patterns in the region are evolving. Starting with the 50th percentile, this parameter shows no significant year-on-year changes across the region. That said, there is a slight general increasing trend in hourly data (except in Mas de Barberans), and more varied behavior at daily scale (though trending towards a decrease). Further evidence of changing precipitation patterns emerges from the analysis of the 95th percentile, which better captures extreme precipitation values. Daily annual data reveal significant increases only in Alcanar, although other stations also exhibit positive trends. This trend is mirrored in hourly observations, where Amposta and Ulldecona demonstrate significant upward trends, with increasing but non-significant trends also observed in La Ràpita and Alcanar. Particularly noteworthy are the autumnal increases in hourly precipitation for both the 50th and 95th percentiles in Amposta and Ulldecona, highlighting a seasonal intensification of rainfall in this area.

This upward trend persists at higher thresholds—exceeding 50 mm/h and up to 90 mm/h for hourly data, as well as 60 mm and 100 mm for

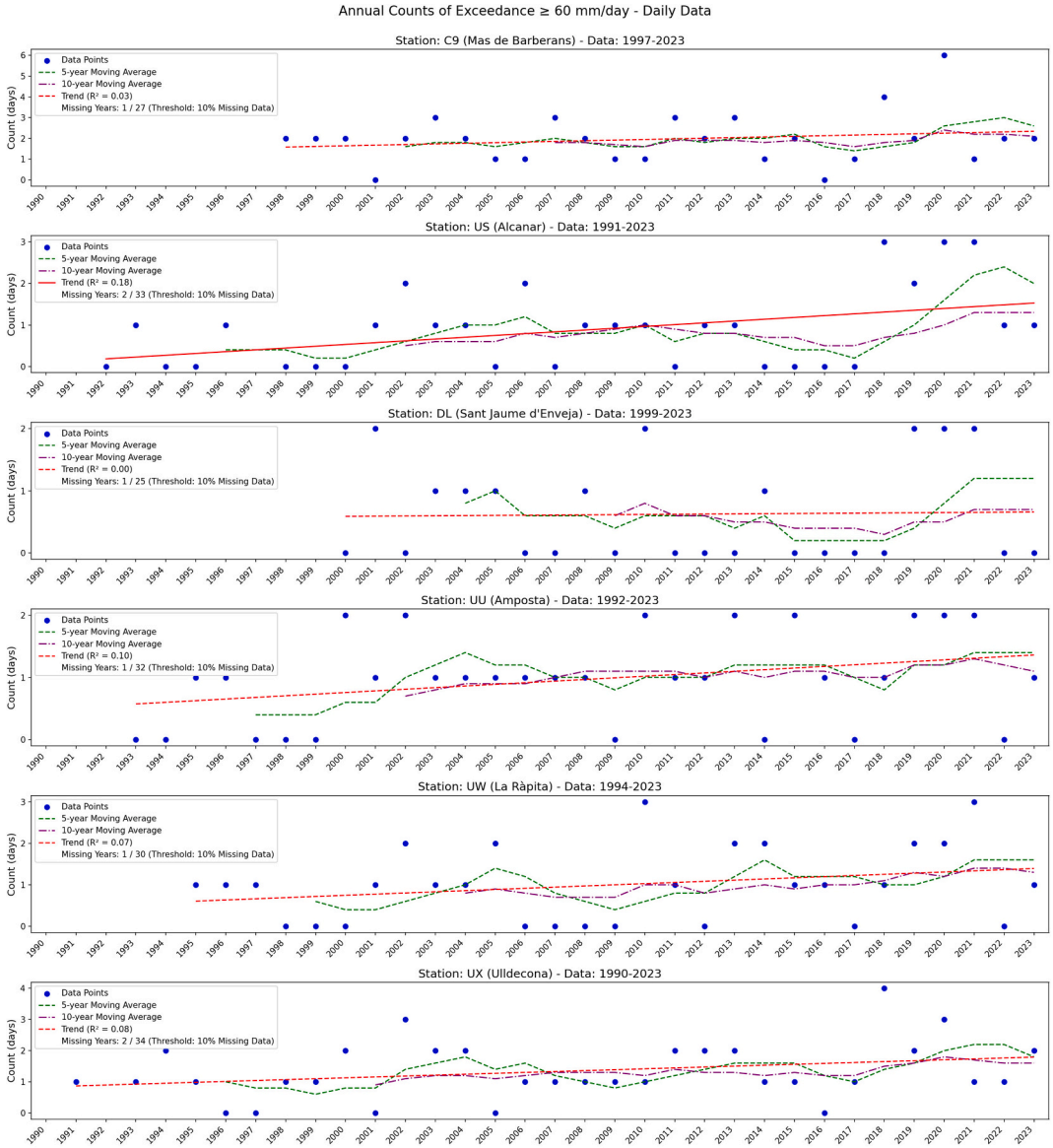

Fig. 22. Annual frequency of precipitation events exceeding 60 mm per day at meteorological stations in Montsià from the early 1990s to 2023. Each subplot corresponds to a distinct station, showing the yearly count of days surpassing this threshold. The dotted green and dash-dot blue lines represent the 5-year and 10-year moving averages, respectively. The red trend line depicts the direction and strength of the trend, with a solid line marking statistical significance at the 95 % confidence level and a dashed line representing a non-significant trend. Stations with more than 10 % missing annual data were excluded, with the number of discarded years specified in each station's legend. (For interpretation of the references to colour in this figure legend, the reader is referred to the web version of this article.)

daily data—with Alcanar consistently exhibiting a significant rise in precipitation events, largely driven by extreme episodes in recent years. At the 60 mm/day threshold, additional increasing trends, though not statistically significant, are observed in Amposta, La Ràpita, and Ulldecona (Fig. 22).

Beyond percentiles, the analysis of kurtosis, skewness, and standard deviation focuses on the internal structure of rainfall variability, highlighting shifts in the frequency of extreme and non-extreme events. For instance, the kurtosis analysis of annual daily precipitation in Alcanar shows a significant increasing trend, indicating a growing tendency towards extreme events. This finding aligns closely with the results from the 95th percentile analysis. Similarly, the analysis of daily skewness further reinforces this picture, because although it does not reveal any significant annual trend, it nonetheless points out an increasing tendency towards more asymmetric precipitation distributions in all the stations except Sant Jaume d'Enveja. The standard deviation of annual daily precipitation values provides additional understanding of variability, with significant positive trends in Amposta and Alcanar, and non-significant but positive trends in La Ràpita and Ulldecona. A seasonal breakdown reveals a marked increase in autumnal standard deviation for Alcanar and La Ràpita, suggesting growing variability during this critical season. When examining hourly precipitation data, the analysis of kurtosis and skewness indicates subtle yet meaningful shift, in distribution shape -pointing to either a flattening or intensification of extreme event distributions, at both annual and seasonal scales. These distributional changes are complemented by the analysis of standard deviation which mirrors the trends found in the daily data. In particular, Alcanar exhibits a significant increase in hourly variability, especially in recent years, emphasizing an intensification of short-duration precipitation events.

6. Discussion

Although not always explicitly addressed, remote sensing has played a key role in analyzing the selected events. Meteosat Second Generation (MSG) water vapor imagery has provided valuable information on the humidity distribution in the mid- and upper levels of the atmosphere and has allowed for improved comparison with outputs from numerical weather prediction models (Georgiev and Martín, 2001). Cloud-to-ground lightning detection maps have also contributed to identifying areas with deep and shallow convective activity (Schultz et al., 2011; Mattos and Machado, 2011). Additionally, various radar products have enabled a detailed forensic analysis of thunderstorms and precipitating systems. These tools have allowed storms to be characterized in terms of vertical extent (echo top), precipitation intensity and type (reflectivity), and cumulative rainfall (via integrated radar volume data), following methodologies similar to those described by Saltikoff et al. (2019) and Smith et al. (2016). In particular, the identification and tracking of convective cores has been definitive for recognizing key structural features throughout the life cycle of the convective systems.

In comparison to other severe convective episodes in Catalonia, total lightning activity in the three events analyzed here was notably lower. For example, the cases presented by Farnell et al. (2017) and Rigo and Farnell (2022) involved strong instability and deep convection, resulting in storms with considerable vertical development and intense lightning activity—features that significantly aided short-term forecasting. In contrast, the present cases were characterized by lower atmospheric instability and shallower convective development, both in terms of storm top and core intensity. These characteristics align more closely with other documented events, such as those analyzed by Del Moral et al. (2020), Farnell and Rigo (2020), and Rigo et al. (2019), which focused on flash floods, lightning activity, and mesoscale convective systems, respectively. In all of these studies, the isozero height (0 °C level) was elevated, and precipitation often remained below this layer. As a result, the cloud systems contained large amounts of precipitable water concentrated in the lower troposphere, leading to intense rainfall rates.

Such cases are commonly classified as highly efficient precipitation systems (Doswell et al., 1996), in contrast to more severe convective storms characterized by hail and high lightning density. The limited vertical development in these events inhibits the formation of frozen hydrometeors, and thus, electrical activity is generally weak. However, when large quantities of moisture are available, and the convective system remains stationary—or when new convective cells repeatedly form over the same area—the accumulated rainfall can reach exceptional levels. This was precisely the situation observed in Montsià, illustrating the mechanisms described by Doswell et al. (1996).

Finally, our analysis of moisture sources is consistent with the findings of Insua-Costa et al. (2018, 2022), who identified the Mediterranean Sea as a key, though not exclusive, contributor to heavy precipitation events in the region. However, as in the cases analyzed here, they also demonstrated that it is not a dominant source, as its contribution generally accounts for less than half of the total recorded precipitation. Our results also agree in highlighting that the accumulation of smaller contributions from multiple sources plays a decisive role in fueling heavy rainfall.

7. Conclusions

This study presents a comprehensive analysis of flash floods in Montsià County (southern Catalonia), with particular focus on three recent events in the municipality of Alcanar—a paradigmatic example of a Western Mediterranean coastal area exposed to extreme rainfall. Between 1996 and 2023, 54 flood episodes were recorded in Montsià, 31 of which affected Alcanar, resulting in nearly 15 million $€_{2022}$ in compensation costs. In fact, the three selected case studies—October 2018, September 2021, and September 2023—stand out not only for their severity but also for their disproportionate economic impact. The 2018 and 2023 events alone generated compensation costs around three times greater than the combined total of all flood events in Alcanar between 1996 and 2017. The 2021 event was even more exceptional, surpassing the combined cost of 2018 and 2023 by several times. In all three cases, precipitation exceeded 200 mm in 24 h and 50 mm in just 30 min.

This impact is further supported by aggregated data from meteorological stations across Montsià, which point to concerning rainfall return levels. These range from 112 mm per day for a 2-year return period to 340 mm per day for a 100-year return period, with high hourly intensities reaching 45 mm/h (2-year) and up to 120 mm/h (100-year). Alcanar, in particular, is remarkable for its pronounced tendency towards intense rainfall, with daily levels increasing from 67 mm (2-year) to 285 mm (100-year) and hourly levels reaching 26 mm, 41 mm, and 100 mm for 2-, 5-, and 50-year return periods, respectively.

From a meteorological perspective, intense rainfall episodes in the area are closely associated with persistent easterly/southeasterly flow at low levels and southerly to/south westerly flow at mid to upper levels typically generated by a cold low or cut-off low (COL) positioned southwest of the Iberian Peninsula. An Atlantic-European anticyclone typically reinforces the easterly synoptic flow, contributing to onshore moisture transport through the mid and upper troposphere. This sustained advection contributes to elevated precipitable water values across the region. Radar observations indicate a variety of convective structures—ranging from mesoscale convective systems (MCSs) to smaller convective cells embedded within broader stratiform precipitation— reflecting the synchronization of multi-scale atmospheric processes in producing heavy rainfall. In the three episodes analyzed, however, the dominant mode was that of convective trains. Echo-tops generally remained below 12 km, implying that conditions were not supportive of widespread deep convection. On the other hand, the presence of a higher freezing level contributed to increased rainfall intensity; in other words, the storms were less severe but more efficient in producing precipitation. In each case the three major events analyzed,

the presence of an upper-level jet streak, moderate CAPE values, and high equivalent potential temperatures at low levels supported repeated cell regeneration over the same area.

Although the Mediterranean Sea consistently acts as the primary moisture source, often supplying up to half of the total atmospheric moisture, additional contributions from remote regions—including the North Atlantic, tropical Africa, or even parts of North America—are also essential to explaining the extraordinary precipitation accumulations observed. While each individual long-range sources may contribute only 5–10 % individually, their combined influence represents a substantial portion of the total moisture budget. This highlights the multi-scale and interconnected nature of flash flood events in the Western Mediterranean.

In addition to long-range moisture transport, the region's orographic and coastal features also play a central role in anchoring and intensifying these rainfall events. The Serra del Montsià, together with the warm waters of the Alfacs' Bay, promotes low-level atmospheric instability and contributes to the stationarity of convective systems. These physical characteristics — combined with the steep ravines and complex terrain—, facilitate rapid runoff, thereby amplifying flash flooding processes across the area. Building on the physical drivers of flash flooding, the updated flood database for the area shows a slight but statistically significant upward trend in flood occurrences in Alcanar, with a similar —though not statistically significant— increase across the broader Montsià region. Complementary evidence from precipitation percentiles, threshold exceedances, and statistical indicators such as skewness and kurtosis points to a rise in rainfall variability and higher annual maxima over the past 5–6 years. While these signals do not constitute definitive proof of a permanent climatic shift, they are consistent with climate change projections anticipating more frequent extreme precipitation events in the Mediterranean.

Considering these observed trends and growing rainfall variability, the recurrent and costly nature of flash floods in Alcanar—particularly in 2018, 2021, and 2023—underscores two parallel needs. First, it is advisable to move beyond stationary return-period curves and consider non-stationary extreme-value frameworks that integrate physically relevant covariates, such as Mediterranean SST anomalies, large-scale circulation patterns, and documented shifts in local and remote moisture-source contributions. Second, operational preparedness could be enhanced through a flash-flood early warning chain that couples high-resolution radar, convection-permitting mesoscale modelling, lightning nowcasting and impact-based communication protocols. To ensure the effectiveness of both anticipatory modelling and response mechanisms, however, coordinated governance is essential. Montsià's fragmented hydrographic management—spread across multiple agencies—requires robust inter-agency coordination, particularly given the history of urban expansion into flood-prone areas.

Looking ahead, future research should aim to improve our understanding of how synoptic-scale cut-off lows interact with local orographic features and contribute to multiscale convective processes. Moreover, the effects of climate change, land-use change and anthropogenic modifications to coastal geomorphology merit closer examination, given their potential to either amplify or mitigate flood impacts. Ultimately, robust, and forward-looking adaptation strategies—combining structural and natural defences with strengthened public-awareness—will be fundamental to reduce risk and protect both lives and economic assets in the context of a changing Western Mediterranean climate.

CRediT authorship contribution statement

Maria Carmen Llasat: Writing – review & editing, Writing – original draft, Supervision, Project administration, Methodology, Investigation, Funding acquisition, Formal analysis, Data curation, Conceptualization. **Raül Marcos-Matamoros:** Writing – review & editing, Methodology, Formal analysis, Data curation, Conceptualization. **Ramón Pascual:** Writing – original draft, Methodology, Investigation, Formal analysis, Conceptualization. **Tomeu Rigo:** Writing – original draft, Methodology, Investigation, Formal analysis, Data curation, Conceptualization. **Damián Insúa-Costa:** Writing – original draft, Methodology, Investigation, Formal analysis. **Alfredo Crespo-Otero:** Writing – original draft, Software, Methodology, Investigation, Formal analysis.

Funding

This study has been supported by the Spanish Project C3RiskMed (PID2020-113638RB-C22 funded by MICIU/AEI/10.13039/501100011033) and from the European Union's Horizon 2020 Research and Innovation Programme under grant agreement No 101037193, I-CHANGE. It has also received the support of the AGAUR project 2021SGR01074.

Declaration of competing interest

The authors declare that they have no known competing financial interests or personal relationships that could have appeared to influence the work reported in this paper.

Acknowledgments

We thank Montserrat Llasat-Botija for the updating of information on flood episodes and associated economic damages. One of the coauthors, Raül Marcos-Matamoros, is a Serra Húnter fellow.

We hereby declare that there is no conflict of interest that would prevent or hinder us from publishing in Atmospheric Research.

Data availability

All meteorological data used come from the Meteorological Service of Catalonia and the State Meteorological Agency; data on financial compensation come from the Insurance Compensation Consortium; data required for the calculation of humidity sources come from the ECMWF ERA5 model. All of them are public bodies. Data on flood episodes come from INUNGAMA and can be downloaded from https://agora.ub.edu.

References

AEMET, 2023. Informe sobre el episodio meteorológico de precipitaciones intensas ocasionadas por una DANA durante los días 2, 3 y 4 de septiembre de 2023. https://www.aemet.es/es/conocermas/recursos_en_linea/publicaciones_y_estudios/estudios/detalles/dana_sep_2023 (last consult 30 August 2024).

Alexander, L.V., Zhang, X., Peterson, T.C., et al., 2006. Global observed changes in daily climate extremes of temperature and precipitation. J. Geophys. Res. Atmos. 111, D05109. https://doi.org/10.1029/2005JD006290.

ARCIMIS, 2021. 1 de septiembre de 2021: inundaciones en Toledo y el sur de Madrid. Tiempo y Clima 5 (74), 20–21. Octubre 2021. http://hdl.handle.net/20.500.11765/14148 (last consult 30 August 2024).

Balasch, J.C., Calvet, J., Tuset, J., 2023. Reconstrucción post-evento del flash-flood del 1 de septiembre de 2021 en Les Cases d'Alcanar (Tarragona). Ingeniería del Agua 27 (1), 29–44. https://doi.org/10.4995/ia.2023.18535.

Blenkinsop, S., Fowler, H.J., Barbero, R., et al., 2018. The INTENSE project: using observations and models to understand the past, present and future of sub-daily rainfall extremes. Adv. Sci. Res. 15, 117–126. https://doi.org/10.5194/asr-15-117-2018.

Braud, I., Roux, H., Anquetin, S., Maubourguet, M.M., Manus, C., Viallet, P., Dartus, D., 2010. The use of distributed hydrological models for the Gard 2002 flash flood event: analysis of associated hydrological processes. J. Hydrol. 394 (1–2), 162–181.

Braud, I., Bouvier, C., Branger, F., Delrieu, G., Le Coz, J., Nord, G., Vandervaere, J.-P., Anquetin, S., Adamovic, M., Andrieu, J., Batiot, C., Boudevillain, B., Brunet, P., Carreau, J., Confoland, A., Didon-Lescot, J.-F., Domergue, J.-M., Douvinet, J., Dramais, G., Freydier, R., Gérard, S., Huza, J., Leblois, E., Le Bourgeois, O., Le Boursicaud, R., Marchand, P., Martin, P., Nottale, L., Patris, N., Renard, B., Seidel, J.-L., Taupin, J.-D., Vannier, O., Vincendon, B., Wijbrans, A., 2014. Multi-scale hydrometeorological observation and modelling for flash flood understanding. Hydrol. Earth Syst. Sci. 18, 3733–3761.

Calvo-Sancho, C., Quitián-Hernández, L., Bolgiani, P., González-Alemán, J.J., Santos-Muñoz, D., Martín, M.L., 2023. Assessment of HARMONIE-AROME in the simulation of the convective activity associated to a subtropical transition using satellite data. Atmos. Res. 290. https://doi.org/10.1016/J.ATMOSRES.2023.106794.

Colby, F.P., 1984. Convective inhibition as a predictor of convection during AVE-SESAME II. Mon. Weather Rev. 112, 2239–2252. https://doi.org/10.1175/1520-0493(1984)112<2239:CIAAPO>2.0.CO;2.
Coles, S., 2001. An Introduction to Statistical Modeling of Extreme Values. Springer.
Del Moral, A., Rigo, T., Llasat, M.C., 2018. A radar-based centroid tracking algorithm for severe weather surveillance: identifying split/merge processes in convective systems. Atmos. Res. 213, 110–120.
Del Moral, A., del Carmen Llasat, M., Rigo, T., 2020. Connecting flash flood events with radar-derived convective storm characteristics on the northwestern Mediterranean coast: knowing the present for better future scenarios adaptation. Atmos. Res. 238, 104863.
Doswell, C.A., Brooks, H.E., Maddox, R.A., 1996. Flash flood forecasting: an ingredients-based methodology. Weather Forecast. 11 (4), 560–581.
Faccini, F., Luino, F., Paliaga, G., Roccati, A., Turconi, L., 2021. Flash flood events along the West Mediterranean Coasts: inundations of urbanized areas conditioned by anthropic impacts. Land 10 (6), 620. https://doi.org/10.3390/land10060620.
Farnell, C., Rigo, T., 2020. The lightning jump algorithm for nowcasting convective rainfall in Catalonia. Atmosphere 11 (4), 397.
Farnell, C., Rigo, T., Pineda, N., 2017. Lightning jump as a nowcast predictor: application to severe weather events in Catalonia. Atmos. Res. 183, 130–141.
Ferreira, R.N., 2021. Cut-off lows and extreme precipitation in eastern Spain: current and future climate. Atmosphere 12 (7), 8.
Gaume, E., Borga, M., Llasat, M.C., Maouche, S., Lang, M., Diakakis, M., 2016. Mediterranean extreme floods and flash floods. Into Hydro-meteorological extremes, chapter 3. In: The Mediterranean Region under Climate Change. A Scientific Update (coordinated byAllEnvi), 2016. IRD Éditions Institut de Recherche pour le Développement, Marseille, pp. 133–144. ISBN: 978-2-7099-2219-7.
Georgiev, C.G., Martín, F., 2001. Use of potential vorticity fields, Meteosat water vapour imagery and pseudowater vapour images for evaluating numerical model behaviour. Meteorol. Appl. 8 (1), 57–69.
Hall, J., Arheimer, B., Borga, M., Brázdil, R., Claps, P., Kiss, A., Kjeldsen, T.R., Kriaučiūnienė, J., Kundzewicz, Z.W., Lang, M., Llasat, M.C., Macdonald, N., McIntyre, N., Mediero, L., Merz, B., Merz, R., Molnar, P., Montanari, A., Neuhold, C., Parajka, J., Perdigão, R.A.P., Plavcová, L., Rogger, M., Salinas, J.L., Sauquet, E., Schär, C., Szolgay, J., Viglione, A., Blöschl, G., 2014. Understanding Flood Regime changes in Europe: a state of the art assessment. Hydrol. Earth Syst. Sci. 18, 2735–2772. www.hydrol-earth-syst-sci.net/18/2735/2014/. https://doi.org/10.5194/hess-18-2735-2014.
Hersbach, H., Bell, B., Berrisford, P., Hirahara, S., Horányi, A., Muñoz-Sabater, J., Nicolas, J., Peubey, C., Radu, R., Schepers, D., Simmons, A., Soci, C., Abdalla, S., Abellan, X., Balsamo, G., Bechtold, P., Biavati, G., Bidlot, J., Bonavita, M., De Chiara, G., Dahlgren, P., Dee, D., Diamantakis, M., Dragani, R., Flemming, J., Forbes, R., Fuentes, M., Geer, A., Haimberger, L., Healy, S., Hogan, R.J., Hólm, E., Janisková, M., Keeley, S., Laloyaux, P., Lopez, P., Lupu, C., Radnoti, G., de Rosnay, P., Rozum, I., Vamborg, F., Villaume, S., Thépaut, J.N., 2020. The ERA5 global reanalysis. Q. J. R. Meteorol. Soc. 146, 1999–2049. https://doi.org/10.1002/qj.3803.
Hosking, J.R.M., Wallis, J.R., 1997. Regional Frequency Analysis: An Approach Based on L-Moments. Cambridge University Press.
Insua-Costa, D., Miguez-Macho, G., Llasat, M., 2018. Local and remote moisture sources for extreme precipitation: a study of the two famous 1982 Western Mediterranean episodes. Hydrol. Earth Syst. Sci. Discuss. https://doi.org/10.5194/hess-2018-421-AC1.
Insua-Costa, D., Lemus-Cánovas, M., Miguez-Macho, G., Llasat, M.C., 2021. Climatology and ranking of hazardous precipitation events in the western Mediterranean area. Atmos. Res. 255, 105521.
Insua-Costa, D., Senande Rivera, M., Llasat, M.C., Miguez-Macho, G., 2022. A global perspective on western Mediterranean precipitation extremes. Nat. Part. J. NPJ Clim. Atmosph. Sci. 5, 9. https://doi.org/10.1038/s41612-022-00234-w.
IPCC, 2022. Climate change 2022: impacts, adaptation and vulnerability. In: Pörtner, H.-O., Roberts, D.C., Tignor, M., Poloczanska, E.S., Mintenbeck, K., Alegría, A., Craig, M., Langsdorf, S., Löschke, S., Möller, V., Okem, A., Rama, B. (Eds.), Contribution of Working Group II to the Sixth Assessment Report of the Intergovernmental Panel on Climate Change. Cambridge University Press, Cambridge, UK and New York, NY, USA, p. 3056. https://doi.org/10.1017/9781009325844.
Jansa, A., Alpert, P., Arbogast, P., Buzzi, A., Ivancan-Picek, B., Kotroni, V., Llasat, M.C., Ramis, C., Richard, E., Romero, R., Speranza, A., 2014. MEDEX: a general overview. Nat. Hazards Earth Syst. Sci. 14, 1965–1984.
Katz, R.W., Parlange, M.B., Naveau, P., 2002. Statistics of extremes in hydrology. Adv. Water Resour. 25 (8–12), 1287–1304. https://doi.org/10.1016/S0309-1708(02)00056-8.
Keune, J., Schumacher, D.L., Miralles, D.G., 2022. A unified framework to estimate the origins of atmospheric moisture and heat using Lagrangian models. Geosci. Model Dev. 15, 1875–1898. https://doi.org/10.5194/gmd-15-1875-2022.
Koutsoyiannis, D., 2004. Statistics of extremes and estimation of extreme rainfall: II. Empirical investigation of long rainfall records. Hydrol. Sci. J. 49 (4), 591–610. https://doi.org/10.1623/hysj.49.4.591.54429.
Llasat, M.C., 2009. Chapter 18: Storms and floods. In: Woodward, Jamie (Ed.), The Physical Geography of the Mediterranean Basin. Oxford University Press, pp. 504–531. ISBN: 978–0–19-926803-0.
Llasat, M.C., Llasat-Botija, M., Petrucci, O., Pasqua, A.A., Rosselló, J., Vinet, F., Boissier, L., 2013. Towards a database on societal impact of Mediterranean floods within the framework of the HYMEX project. Nat. Hazards Earth Syst. Sci. 13, 1337–1350. www.nat-hazards-earth-syst-sci.net/13/1/2013/. https://doi.org/10.5194/nhess-13-1-2013.
Llasat, M.C., del Moral, A., Cortès, M., Rigo, T., 2021. Convective precipitation trends in the Spanish Mediterranean region. Atmos. Res. 257 (2021), 10558. https://doi.org/10.1016/j.atmosres.2021.105581.
Mattos, E.V., Machado, L.A., 2011. Cloud-to-ground lightning and Mesoscale Convective Systems. Atmos. Res. 99 (3–4), 377–390.
MedECC, 2020. Climate and environmental change in the Mediterranean Basin – current situation and risks for the future. In: Cramer, W., Guiot, J., Marini, K. (Eds.), First Mediterranean Assessment Report. Union for the Mediterranean, Plan Bleu, UNEP/MAP, Marseille, France, p. 632. https://doi.org/10.5281/zenodo.4768833. ISBN: 978-2-9577416-0-1 17/11/2020. Available at https://www.medecc.org/medecc-reports/climate-and-environmental-change-in-the-mediterranean-basin-current-situation-and-risks-for-the-future-1st-mediterranean-assessment-report/ (last consult 13 March 2025).
Moncrieff, M.W., Miller, M.J., 1976. The dynamics and simulation of tropical cumulonimbus and squall lines. QJR Meteorol. Soc. 102, 373–394. https://doi.org/10.1002/qj.49710243208.
Mudelsee, M., 2010. Climate Time Series Analysis: Classical Statistical and Bootstrap Methods, 2nd ed. Springer. https://doi.org/10.1007/978-90-481-9482-7.
Najibi, N., Devineni, N., 2018. Recent trends in the frequency and duration of global floods. Earth Syst. Dynam. 9 (2), 757–783. https://doi.org/10.5194/esd-9-757-2018.
NOAA, 2006. Precipitation Frequency Atlas of the United States: NOAA Atlas 14 (Vol. 2, Version 3.0, § 4.5). NOAA/NWS.
Papalexiou, S.M., Koutsoyiannis, D., 2013. Battle of extreme value distributions: a global survey on extreme daily rainfall. Water Resour. Res. 49 (1), 187–201. https://doi.org/10.1029/2012WR012557.
Pisso, I., Sollum, E., Grythe, H., Kristiansen, N.I., Cassiani, M., Eckhardt, S., Arnold, D., Morton, D., Thompson, R.L., Groot Zwaaftink, C.D., Evangeliou, N., Sodemann, H., Haimberger, L., Henne, S., Brunner, D., Burkhart, J.F., Fouilloux, A., Brioude, J., Philipp, A., Seibert, P., Stohl, A., 2019. The Lagrangian particle dispersion model FLEXPART version 10.4. Geosci. Model Dev. 12, 4955–4997. https://doi.org/10.5194/gmd-12-4955-2019.
Poncet, N., Lucas-Picher, P., Tramblay, Y., Thirel, G., Vergara, H., Gourley, J., Alias, A., 2024. Does a convection-permitting regional climate model bring new perspectives on the projection of Mediterranean floods? Nat. Hazards Earth Syst. Sci. 24, 1163–1183. https://doi.org/10.5194/nhess-24-1163-2024.
Reboita, M.S., Mattos, E.V., Capucin, B.C., Souza, D.O., Ferreira, G.W.D.S., 2024. A multi-scale analysis of the extreme precipitation in Southern Brazil in April/May 2024. Atmosphere 15 (9), 1123. https://doi.org/10.3390/atmos15091123.
Rigo, T., Farnell, C., 2022. Characterisation of thunderstorms with multiple lightning jumps. Atmosphere 13 (2), 171.
Rigo, T., Llasat, M.C., 2004. A methodology for the classification of convective structures using meteorological radar: Application to heavy rainfall events on the Mediterranean coast of the Iberian Peninsula. Nat. Hazards Earth Syst. Sci. 4 (1), 59–68.
Rigo, T., Llasat, M.C., 2016. Forecasting hailfall using parameters for convective cells identified by radar. Atmos. Res. 169, 366–376.
Rigo, T., Berenguer, M., Llasat, M.C., 2019. An improved analysis of mesoscale convective systems in the western Mediterranean using weather radar. Atmos. Res. 227, 147–156.
Romero, R., Sumner, G., Ramis, C., Genovés, A., 1999. A classification of the atmospheric circulation patterns producing significant daily rainfall in the Spanish Mediterranean area. Int. J. Climatol. 19, 765–785.
Saltikoff, E., Haase, G., Delobbe, L., Gaussiat, N., Martet, M., Idziorek, D., Leijnse, H., Novák, P., Lukach, M., Stephan, K., 2019. OPERA the radar project. Atmosphere 10 (6), 320. https://doi.org/10.3390/atmos10060320.
Sauquet, R., Aguilella, A., Macià, N., Castiñeira, I., 2023. Study of architectural, urban, and landscape solutions to mitigate the effects of heavy rainfall in the municipality of Alcanar [Internal scientific-technical report, originally in Catalan]. Centre for Research in Local Administration (CRAL). & HABITAR Research Group. Universitat Politècnica de Catalunya.
Schultz, C.J., Petersen, W.A., Carey, L.D., 2011. Lightning and severe weather: a comparison between totaland cloud-to-ground lightning trends. Weather Forecast. 26 (5), 744–755.
Smith, T.M., Lakshmanan, V., Stumpf, G.J., Ortega, K.L., Hondl, K., Cooper, K., Calhoun, K.M., Kingfield, D.M., Manross, K.L., Toomey, R., Brogden, J., 2016. Multi-radar multi-sensor (MRMS) severe weather and aviation products: initial operating capabilities. Bull. Am. Meteorol. Soc. 97 (9), 1617–1630. https://doi.org/10.1175/BAMS-D-14-00173.1.
Sodemann, H., Schwierz, C., Wernli, H., 2008. Interannual variability of Greenland winter precipitation sources: Lagrangian moisture diagnostic and North Atlantic Oscillation influence. J. Geophys. Res. Atmos. 113, D03107. https://doi.org/10.1029/2007JD008503.
Stephens, M.A., 1974. EDF statistics for goodness of fit and some comparisons. J. Am. Stat. Assoc. 69 (347), 730–737. https://doi.org/10.1080/01621459.1974.10480196.
Stohl, A., James, P.A., 2004. Lagrangian analysis of the atmospheric branch of the global water cycle. Part I: method description, validation, and demonstration for the August 2002 flooding in Central Europe. J. Hydrometeorol. 5, 656–678. https://doi.org/10.1175/1525-7541(2004)005%3C0656:ALAOTA%3E2.0.CO;2.
Tramblay, Y., Somot, S., 2018. Future evolution of extreme precipitation in the Mediterranean. Clim. Chang. 151, 289–302. https://doi.org/10.1007/s10584-018-2300-5.
Tramblay, Y., Mimeau, L., Neppel, L., Vinet, F., Sauquet, E., 2019. Detection and attribution of flood trends in Mediterranean basins. Hydrol. Earth Syst. Sci. 23 (11), 4419–4431. https://doi.org/10.5194/hess-23-4419-2019.

Treppiedi, D., Cipolla, G., Francipane, A., Noto, L.V., 2021. Detecting precipitation trend using a multiscale approach based on quantile regression over a Mediterranean area. Int. J. Climatol. 1–18. https://doi.org/10.1002/joc.7161.

Uccellini, L.W., Johnson, D.R., 1979. The coupling of Upper and Lower Tropospheric jet streaks and implications for the development of severe convective storms. Mon. Weather Rev. 107, 682–703. https://doi.org/10.1175/1520-0493(1979)107<0682:TCOUAL>2.0.CO;2.

United Nations, 2023. The United Nations World Water Development Report 2023: Partnerships and Cooperation for Water. UNESCO, Paris. Available at https://www.unwater.org/publications/un-world-water-development-report-2023 (last consult 21 August 2024).

Westra, S., Fowler, H.J., Evans, J.P., et al., 2014. Future changes to the intensity and frequency of short-duration extreme rainfall. Rev. Geophys. 52, 522–555. https://doi.org/10.1002/2014RG000464.

Wilks, D.S., 2011. Statistical Methods in the Atmospheric Sciences, 3rd ed. Academic Press.

WMO, 1989. Statistical Distributions for Flood Frequency Analysis (Operational Hydrology Report No. 33, Ch. 6). WMO.

WMO, 2023. Early Warnings For All. The UN Global Early Warning Initiative for the implementation of Climate Adaptation. Executive Action Plan 2023–2027 Initiative Scaled up into Action on the Ground. Available at https://library.wmo.int/records/item/58209-early-warnings-for-all.